



HAL
open science

Live Imaging Reveals Listeria Hijacking of E-Cadherin Recycling as It Crosses the Intestinal Barrier

Minhee Kim, Cindy Fevre, Morgane Lavina, Olivier Disson, Marc Lecuit

► **To cite this version:**

Minhee Kim, Cindy Fevre, Morgane Lavina, Olivier Disson, Marc Lecuit. Live Imaging Reveals Listeria Hijacking of E-Cadherin Recycling as It Crosses the Intestinal Barrier. *Current Biology - CB*, 2021, 31 (5), pp.1037-1047.e4. 10.1016/j.cub.2020.11.041 . pasteur-03271351

HAL Id: pasteur-03271351

<https://pasteur.hal.science/pasteur-03271351>

Submitted on 25 Jun 2021

HAL is a multi-disciplinary open access archive for the deposit and dissemination of scientific research documents, whether they are published or not. The documents may come from teaching and research institutions in France or abroad, or from public or private research centers.

L'archive ouverte pluridisciplinaire **HAL**, est destinée au dépôt et à la diffusion de documents scientifiques de niveau recherche, publiés ou non, émanant des établissements d'enseignement et de recherche français ou étrangers, des laboratoires publics ou privés.



Distributed under a Creative Commons Attribution - NonCommercial 4.0 International License

1 **Live imaging reveals *Listeria* hijacking of E-cadherin recycling as it crosses**
2 **the intestinal barrier**

3

4

5 Minhee Kim^{1,2}, Cindy Fevre^{1,2}, Morgane Lavina^{1,2}, Olivier Disson^{1,2,#}, Marc Lecuit^{1,2,3,4#,*}

6

7

8 ¹ Institut Pasteur, Biology of Infection Unit, Paris, France

9 ² Inserm U1117, Paris, France

10 ³ Université de Paris, Necker-Enfants Malades University Hospital, Division of Infectious
11 Diseases and Tropical Medicine, Institut Imagine, APHP, Paris, France

12 ⁴ Institut Universitaire de France (IUF)

13

14

15 # O.D. and M.Lecuit share senior authorship

16 * Corresponding author and lead contact: marc.lecuit@pasteur.fr (M.Lecuit)

17 **SUMMARY**

18 *Listeria monocytogenes* is a foodborne bacterial pathogen that causes human listeriosis, a
19 severe systemic infection [1]. Its translocation across the intestinal epithelium is mediated by
20 the interaction of internalin (InlA), a *Listeria* surface protein, with its host species-specific
21 receptor E-cadherin (Ecad) [2-5]. It occurs through goblet cells, on which Ecad is lumenally
22 accessible [6], *via* an unknown mechanism. In the absence of cell lines recapitulating this
23 phenotype *in vitro*, we developed an *ex vivo* experimental system, based on the intraluminal
24 microinjection of *Listeria* in untreated, pharmacologically-treated and genetically modified
25 intestinal organoids. Using both live light sheet microscopy and confocal imaging, we show
26 that *Listeria* translocates through goblet cells within a membrane vacuole in an InlA- and
27 microtubule-dependent manner. As Ecad undergoes constant apical-basal recycling [7, 8], we
28 hypothesized that *Lm* may transit through goblet cells by hijacking Ecad recycling pathway.
29 Indeed, *Listeria* is stuck at goblet cell apex when Ecad endocytosis is blocked, and remains
30 trapped intracellularly at the basolateral pole of goblet cells when Rab11-dependent Ecad
31 recycling is compromised. Together, these results show that *Listeria*, upon docking onto its
32 lumenally accessible receptor Ecad, hijacks its recycling pathway to be transferred by
33 transcytosis across goblet cells. Live imaging of host-pathogen interactions in organoids is a
34 promising approach to dissect their underlying cell and molecular biology.

35

36

37 **Keywords**

38 *Listeria*, epithelial translocation, organoids, intestine, goblet cell, E-cadherin recycling, live
39 imaging, Rab11

40

41 RESULTS AND DISCUSSION

42 In order to decipher the cell biology mechanisms of *Listeria* translocation across the intestinal
43 epithelium, we developed a genetically amenable experimental system permissive to InlA-
44 Ecad-dependent trans-epithelial crossing. Deciphering the detailed cell biology mechanisms
45 of *Listeria* translocation across the intestinal epithelium *in vivo* would require interfering with
46 cellular pathways that may disrupt its barrier function. Additionally, it would be extremely
47 challenging to capture *Listeria* translocation in real-time across intestinal villus epithelium,
48 given its rarity and intestinal peristalsis. Furthermore, no adherent cell, including human
49 colonic cell lines T84, HT29 and Caco-2, displays an apical-basal polarization and apical
50 accessibility of Ecad, which are both critical for *Listeria* InlA-Ecad-dependent trans-epithelial
51 crossing to occur (our unpublished observations). We therefore set up an *ex vivo* experimental
52 system based on the microinjection of *Listeria* in the lumen of intestinal organoids. Intestinal
53 organoids derive clonally from intestinal stem cells, which give rise to a fully differentiated,
54 polarized intestinal epithelium that forms a so-called “minigut” centered by a lumen, and
55 contains differentiated intestinal cell subtypes [9]. Intestinal organoids are genetically
56 amenable [10-13], can be subjected to pharmacological interventions [14], and can also be
57 imaged both fixed and alive [9, 15].

58 59 Intestinal organoids contain goblet cells

60 We generated intestinal organoids from the small intestine of knock-in E16P (E16P KI) mice,
61 in which the endogenous mouse Ecad is punctually modified to express a proline at position
62 16 of the mature protein in place of a glutamic acid. This modification enables this
63 “humanized” mouse Ecad to interact with InlA and mediate *Listeria* internalization [1, 4, 16]
64 (see Methods). As expected [9], E16P organoids grown in Matrigel[®] exhibit a fully mature
65 apical-basal polarity and display cell subtype heterogeneity. Organoids intestinal stem cells
66 differentiate into enterocytes (Villin⁺), enteroendocrine cells (ChromograninA⁺), goblet cells
67 (WGA⁺/Lysozyme^{low}) and Paneth cells (WGA^{low}/Lysozyme⁺, Figure S1A). Additionally, and
68 as previously reported [17], intestinal organoids do not contain M cells (GP2⁺) (Figure S1A).
69 As *Listeria* cross the intestinal barrier via goblet cells *in vivo*, it is important to
70 unambiguously identify this cell subtype in our experimental model. Goblet cells are mucus-
71 secreting cells with a characteristic goblet-shaped cell morphology, which nucleus location
72 does not align with neighboring enterocytes [18]. Additionally, goblet cells can be identified
73 by immunolabeling of the Muc2 mucin, a major mucus component, following Carnoy
74 hydrophobic fixation [19]. However, Muc2 labeling cannot be applied to our experimental

75 system: Carnoy fixation damages plastic wells in which Matrigel® embedded organoids are
76 located, and more importantly, renders Matrigel® opaque. Therefore, we used wheat germ
77 agglutinin (WGA), which labels mucus by binding to sialic acid and N-acetyl-glucosaminyl
78 carbohydrate residues on mature, modified mucins [20, 21]. WGA positive cells were co-
79 labeled for cytokeratin-18, which is specifically expressed in goblet cells in the gut [22]
80 (Figure S1B). Of note, PFA fixation can dissolve mucus, resulting in bona-fide WGA-
81 negative goblet cells. Therefore, we used the following criteria to identify goblet cells: (i)
82 WGA labeling, (ii) goblet-shaped cellular morphology, and (iii) misaligned nucleus relative to
83 neighboring cells. When WGA-negative cells strictly met the last two conditions, we also
84 considered them as goblet cells (e.g., in Figure S1D right).

85

86 ***Listeria* translocation across intestinal organoid goblet cells requires InlA**

87 We microinjected 5×10^3 CFUs of wild type *Lm* into the lumen of mature organoids and
88 investigated bacteria interactions with the intestinal epithelium (Figure 1A). Confocal imaging
89 of intestinal organoids fixed 1 hour after microinjection allowed the detection of bacteria both
90 inside and underneath the basolateral pole of goblet cells (Figure 1B, Video S1).
91 Quantification studies 16 hours post-infection revealed that bacteria were all located exterior
92 to microinjected organoids, specifically associated with goblet cells, as a result of
93 translocation events (Figure 1C). Of note, the microinjection procedure and/or presence of
94 bacteria in the organoid lumen did not modify the proportion of WGA⁺ cells (10.87 ± 3.07 %)
95 compared to non-injected organoids (9.56 ± 2.62 %, Figure S1C). Consistent with our
96 previous *in vivo* studies in humanized mice permissive to InlA-Ecad interaction [5, 6, 16], this
97 phenotype was strictly InlA-dependent. In contrast, it was independent of LLO and ActA,
98 which mediate *Lm* escape from its internalization vacuole and actin-based motility,
99 respectively (Figure 1C). *Li*(InlA) is derived from *L. innocua*, a non-pathogenic *Listeria*
100 species devoid of *L. monocytogenes* virulence factors, which has been genetically modified to
101 express InlA, and enters into cells in an Ecad-dependent manner [23]. Upon microinjection in
102 intestinal organoids lumen, *Li*(InlA) was also located extracellularly at basolateral pole of
103 goblet cells, as wild type *Lm* (Figure 1C, Figure S1D,E, Video S1). This indicates that
104 *Listeria* crossing of the intestinal epithelium does not require escape from the vacuole and
105 actin-based motility. In some cases, bacteria underneath goblet cells were surrounded with
106 WGA-labeled material, implying that bacteria can translocate with mucus (Figure S1E). Of
107 note, bacteria beneath goblet cells cannot replicate or move within Matrigel®, as it contains
108 gentamicin and is bactericidal. Together, these results show that *Listeria* microinjection in the

109 lumen of intestinal organoids allows to faithfully recapitulate *Listeria* translocation across the
110 intestinal epithelium *in vivo*. These results also confirm that InlA is necessary and sufficient to
111 mediate *Listeria* translocation across goblet cells, while LLO and ActA are dispensable [6],
112 and justify the use of *Li*(InlA) for further experiments, in order to minimize the potential
113 cytotoxicity of LLO to microinjected organoids [24].

114

115 **Real-time imaging of *Listeria* transcytosis across intestinal organoid epithelium**

116 Despite converging evidences indicating that *Listeria* transcytoses through goblet cells *in vivo*
117 [6], live imaging has not been performed to prove it actually occurs, *i.e.* translocation of a
118 bacterium surrounded by its internalization vacuole. We therefore set up experimental
119 conditions to image in real time translocation of *Li*-GFP(InlA) across intestinal organoids in
120 which cell membranes are constitutively red fluorescent (mtd-Tmt; E16P KI). *Listeria*
121 translocation across the intestinal epithelium is a rare event *in vivo*, as only 3 to 4% of
122 intestinal villi are infected in 45 minutes long intestinal ligated loop assays (our unpublished
123 observation). Moreover, *Lm* translocation across the small intestinal epithelium occurs within
124 30 minutes *in vivo* [6]. The rarity of translocation events requires that entire organoids are
125 scanned to be captured, and this may exceed the time needed for bacterial translocation when
126 using classical confocal imaging. Additionally, laser power has to be minimal to preserve the
127 fluorescence signal of individual bacteria and cell membrane over prolonged imaging.
128 Furthermore, imaging has to be performed at the adequate spatial resolution to track micron-
129 sized bacteria within intestinal organoids, the diameter of which ranges from hundreds to
130 thousands of microns. To accommodate all these experimental requirements, light sheet
131 microscopy was used, which can image intestinal organoids at least thirty times faster than a
132 regular confocal microscope with minimal phototoxicity. 5×10^3 CFUs of *Li*-GFP(InlA) were
133 microinjected intraluminally into mtd-Tmt; E16P KI organoids. Real time imaging revealed
134 that a bacterium reached cell basolateral pole surrounded by a cell membrane in less than 12
135 minutes. During the following 36 minutes, the bacterium remained at the basolateral pole of
136 the cell, surrounded by mtd-Tmt signal, and then exited from the cell basolaterally (Figure
137 1D, Video S2). This allowed to image for the first time *Listeria* transcytosis across the
138 intestinal epithelium directly and unambiguously.

139

140 **Ecad is lumenally accessible on goblet cells in intestinal organoids**

141 InlA-dependent translocation of *Listeria* specifically through goblet cell (Figure 1B,C, Figure
142 S1D,E) suggests that translocation is mediated by InlA interaction with lumenally accessible

143 Ecad on goblet cells, as it has been observed *in vivo* [6]. To assess luminal accessibility of
144 Ecad in organoids, we applied an Ecad antibody directed against its ectodomain (ECCD-2) to
145 the accessible luminal side of fixed and sectioned organoids (Figure 1E). To stain only
146 accessible Ecad, we performed surface immunolabeling without cell permeabilization.
147 Junctional proteins in the sectioned plane are exposed, accessible without permeabilization,
148 and are therefore also labeled. However, junctional proteins located below the cutting plane
149 cannot be labeled in the absence of cell permeabilization, unless they are inherently lumenally
150 accessible (Figure 1E,F). As expected given the specific location of InlA-Ecad *Listeria*
151 translocation (Figure 1C), lumenally accessible Ecad was detected only on the apical side of
152 mucus-expelling goblet cells in non-permeabilized organoids (Figure 1E, Video S3). In
153 contrast, in permeabilized organoids, Ecad was detected at *adherens* junctions, down to the
154 basolateral membrane in all cells regardless of the subtype (Figure 1F, Video S3). Together,
155 these results indicate that the cells on which Ecad is lumenally accessible in intestinal
156 organoids are mucus-expelling goblet cells, and that bacteria located beneath the basal pole of
157 goblet cells after intraluminal microinjection have undergone InlA-Ecad-mediated
158 transcytosis. This establishes the specificity of this *ex vivo* experimental system to study the
159 cell biology of *Listeria* InlA-Ecad translocation across the intestinal epithelium.

160

161 **Endocytosis and microtubule dynamics are required for *Listeria* translocation through** 162 **goblet cells**

163 Previous *in vivo* investigations have shown that InlA-Ecad-dependent *Listeria* crossing of the
164 intestinal barrier depends on microtubule and the exocytic machinery [6]. We therefore
165 hypothesized that *Listeria*, upon its docking on lumenally accessible Ecad on goblet cells,
166 hijacks Ecad recycling pathway to cross the intestinal epithelial barrier, from its dynamin-
167 mediated endocytosis [7] and endosomal trafficking along microtubules [25], to its Rab11
168 dependent release at the cell basolateral pole [26, 27]. Ecad recycling has not been studied in
169 goblet cells, but it is also expected to involve its endocytosis at the apical pole and basolateral
170 recycling in a microtubule-dependent manner. We therefore tested this hypothesis by
171 dissecting the role of Ecad recycling pathway on *Listeria* transcytosis.

172 In polarized differentiated cells, Ecad, which forms *adherens* junctions (AJ), is endocytosed
173 in a clathrin-dependent manner [7]. The resulting endosomes are excised from the plasma
174 membrane by the GTPase dynamin [28, 29]. Ecad is trafficked in a microtubule-dependent
175 manner [25, 30, 31] and recycled to the basolateral membrane [7]. To first inhibit Ecad
176 endocytosis, we used dynasore, a dynamin inhibitor that prevents the fission of clathrin- and

177 caveolin-dependent endocytic vacuoles [32, 33]. To inhibit microtubule-based Ecad
178 trafficking, we used colchicine, which blocks microtubule polymerization. In organoids
179 treated 2 hours with dynasore, cytosolic endocytic Ecad *punctae* were drastically reduced
180 (Figure S2C), as previously reported in cultured cells [29]. In presence of colchicine, more
181 cells with metaphase-blocked mitoses were observed (Figure 2A) as expected [34], indicating
182 that both drugs are active in our system. Nevertheless, the overall morphology and polarity of
183 the organoids were comparable to non-treated controls (Figure 2A) and we observed no
184 difference in total bacterial association to cells (either apically, intracellularly or basolaterally)
185 (Figure 2B). Yet there was a significant decrease of extracellular translocated bacteria in
186 dynasore- and colchicine-treated organoids, relative to control organoids (Figure 2C).
187 Consistent with a similar total bacterial association to cells in all conditions, accessible Ecad
188 was detected similarly on goblet cells in dynasore- and colchicine-treated conditions (Figure
189 2D, Figure S2, Video S4), as in untreated organoids (Figure 1E). This suggests that the
190 interaction between *Listeria* and its receptor Ecad is not impaired in dynasore- and colchicine-
191 treated organoids, whereas *Listeria* transcellular transport is blocked within goblet cells. To
192 examine where bacteria were trapped in cells, we investigated their location in three distinct
193 compartments: apically associated to the cell membrane, intracellular, and extracellular at
194 their basal pole. In dynasore-treated organoids, bacteria were mostly apically associated
195 (Figure 2C,E dynasore, Figure S3, Video S4). These bacteria were likely trapped in elongated
196 invaginations of the plasma membrane, as observed both in *Drosophila* and mammalian
197 epithelial cells when dynamin is inhibited [35-37]. In colchicine-treated organoids, where
198 microtubule dynamics is inhibited, intracellular bacteria were located in the median part of the
199 cells (Figure 2C,E colchicine, Figure S3, Video S4). In all experimental conditions,
200 intracellular bacteria were surrounded with Tomato red-labelled membrane, indicating that
201 bacteria were within a vacuole (Figure 2E). Together, these results show that upon InlA-
202 mediated *Listeria* docking to Ecad, Ecad endocytosis is required to complete bacterial
203 internalization into goblet cells, and microtubules dynamics is required for bacterial trans-
204 epithelial transit in a vacuole.

205

206 **Rab11 is required to complete *Listeria* intestinal translocation through goblet cells**

207 We next investigated whether recycling of Ecad endosomes is required for *Listeria* InlA-
208 dependent translocation across the intestinal epithelium. Ecad is recycled and trafficked *via*
209 Rab11-positive recycling endosomes, which recruit the exocytosis machinery [8, 26, 27, 38,
210 39]. Rab11 is also involved in basolateral sorting of newly synthesized Ecad in polarized

211 mammalian cells *in vitro* [38]. The kinetics of Rab11-based trafficking is around 30 minutes
212 [40, 41], which fits with our live imaging of *Listeria* crossing the epithelium (Figure 1D and
213 Videos S2). Therefore, to perturb Ecad recycling, we targeted Rab11. Since Rab11 null
214 mutations are embryonically lethal in mice [42, 43] and constitutive knock-out of Rab11 may
215 be detrimental for the development of intestinal organoids, we generated lentivirus-transduced
216 organoids in which a dominant negative and myc-tagged version of Rab11 can be induced by
217 doxycycline. As Rab7-dependent Ecad degradation pathway [44] is not expected to be
218 involved in bacterial translocation, we also generated lentivirus-transduced organoids in
219 which a dominant negative Rab7 can be induced, to use them as negative controls. To
220 visualize successful transduction and transcription induction, we used a bi-cistronic reporter
221 system where an internal ribosome entry site (IRES) is placed downstream of each DN mutant
222 and upstream of a mCerulean coding sequence (Figure 3A,B). Organoids were grown and
223 maintained in presence of antibiotics to select for transduced cells. When organoids were
224 properly formed and mature, doxycycline was added 12-16 hours before microinjection to
225 induce the transcription of dominant negative Rab11 and Rab7 variants Rab11DN and
226 Rab7DN, respectively (Figure 4A). Organoids expressing Rab11DN exhibited cytosolic Ecad
227 *punctae* that accumulated at basolateral side of epithelial cells compared to control organoids,
228 consistent with a blockade of Ecad release when Rab11 is non-functional (Figure S2C).
229 Induced expression of Rab7DN caused general enrichment of cytosolic Ecad (Figure S2C),
230 and large Ecad aggregates formed throughout the apical-basal axis (Figure S2C), suggesting
231 that Ecad degradation is affected when Rab7 is non-functional [44]. However, inducing
232 Rab11 and Rab7 dominant negative proteins for a short period of time (less than 24 hours) did
233 not detectably impair epithelium morphology (Figure 3C) and Ecad luminal accessibility
234 compared to WT organoids (Figure 4B, Figure S2, Videos S5).

235 Microinjection experiments revealed that induction of Rab7DN did not affect bacterial
236 translocation through goblet cells. *Listeria* was found extracellular at the basolateral pole of
237 goblet cells of Rab7DN-induced organoids, to the same degree than in transduced but non-
238 induced control organoids (NI). This shows that bacteria complete translocation normally
239 within goblet cells in presence of Rab7DN (Figure 4C-E Rab7DN, Figure S3, Video S5). In
240 contrast, in mycRab11DN-induced transduced organoids, a significant decrease of
241 translocated bacteria beneath goblet cells was observed, together with a corresponding
242 significant increase of intracellular bacteria. Intracellular bacteria were mostly located at the
243 basolateral pole of goblet cells (Figure 4C-E Rab11DN, Figure S3, Video S5). This was also
244 the case for wild type *Listeria* microinjected in mycRab11DN-induced organoids, even 16-

245 hour post microinjection (Figure S2D-F). Note that prolonged exposure to doxycycline might
246 have prevented *Listeria* vacuolar escape and cell-to-cell spread at this late time point. Taken
247 together, these data show that Rab11, in contrast to Rab7, is required for the release of
248 bacteria from the basal pole of goblet cells, highlighting that *Listeria* hijacks Rab11-
249 dependent Ecad recycling for trans-epithelial translocation *via* goblet cells.

250

251 **Organoid as a model for real-time investigation of host-pathogen interactions**

252 Here, we have developed an *ex vivo* minigut system in which *Listeria* crosses the intestinal
253 barrier by transcytosis through goblet cells as it does *in vivo* [6]. We have harnessed the
254 power of this experimental system to directly image, in real time, the trans-epithelial
255 translocation of a microbial pathogen, and to dissect the underlying cell biology and
256 molecular mechanisms. *Listeria* crossing of the intestinal barrier relies on the specific
257 interaction of InlA with lumenally accessible Ecad at the apical pole of goblet cells. We have
258 shown that (i) bacterial Ecad-dependent internalization in goblet cells requires dynamin-
259 mediated endocytosis, (ii) bacteria transit through these cells in a microtubule-dependent
260 manner as *in vivo* [6], and (iii) Rab11 is required for the release of *Listeria* at the basolateral
261 pole of goblet cells, thereby showing that *Listeria* hijacks E-cadherin recycling pathway to
262 cross the intestinal barrier (Figure S3). While organoids have been used to investigate
263 infection with human norovirus and SARS-CoV-2 [45, 46], and the interactions of
264 enteropathogens such as *Salmonella enterica* [47] and *Cryptosporidium parvum* with the
265 intestinal epithelium [48], here we have microinjected for the first time microbes in the lumen
266 of intestinal organoids, imaged in real time microbial crossing of the intestinal barrier, and
267 deciphered the underlying molecular mechanisms of microbial translocation. This novel *ex*
268 *vivo* system of infection opens a wide range of opportunities to study pathogen interactions
269 with host barriers in a direct manner, in contrast to what has been done so far. Additionally,
270 this study also pioneers the use of genetically modified inducible organoids to address the
271 cellular and molecular mechanisms of host-pathogen interactions in a tissue context. Rab11
272 has been shown to be necessary for Ecad recycling in mammalian cells and *in vivo* in
273 *Drosophila melanogaster* [8]. Moreover, Rab11 is required for basolateral trafficking of
274 newly synthesized Ecad in polarized MDCK cells [38]. However, the cellular trafficking of
275 Ecad from its apical to basolateral pole from either side of *adherens* junctions had not been
276 thoroughly investigated in a tissue context to our knowledge. It has been previously shown in
277 non-polarized epithelial intestinal Caco-2 and trophoblastic JEG3 cell lines that, upon binding
278 of InlA to Ecad, the plasma membrane is remodeled in an actin-dependent manner and leads

279 to caveolin- and clathrin-dependent bacterial endocytosis [32, 49-53]. In cultured epithelial
280 cells, *Listeria* internalization occurs mainly at the edge of cell islets, where cells are non-
281 polarized and Ecad is broadly accessible. Once internalized into these non-polarized cells, *Lm*
282 escapes from the vacuole in an LLO dependent manner and propels itself through ActA in the
283 cytosol [54]. Here, we have shown that in polarized differentiated goblet cells in a tissue
284 context, the initial step of internalization through accessible Ecad is also dynamin-dependent.
285 However, after completing bacterial internalization, *Lm* is rapidly transferred and released to
286 the basolateral pole of goblet cells, owing to the rapid Rab11-dependent recycling of Ecad.
287 This may protect invading bacteria from epithelial innate immune responses and favor their
288 dissemination in host tissues. Live imaging of host-pathogen interactions in organoids is a
289 promising approach to dissect their underlying cell and molecular biology.

290 **Acknowledgements**

291 We thank Dr. Thaddeus Stappenbeck, Washington University in Saint Louis, USA and
292 Corinne Lebreton, Institut Imagine, Paris, France for the L-WRN cell line. We thank Miranda
293 Vogt, Stanford University, USA, for her contribution to this study as a summer student. We
294 thank for the help of Image Analysis Hub of the Institut Pasteur and the members of Biology
295 of Infection Unit for their support. Minhee Kim received a long-term postdoctoral fellowship
296 from the European Molecular Biology Organization (EMBO), ALTF 1192-2017. Institut
297 Pasteur, Inserm, LabEx IBEID, the European Research Council (ERC) Invadis and ANR
298 Organolist provided financial support.

299

300 **Authors' contributions**

301 M. Lecuit conceived the project, designed the study, directed the research and edited the
302 manuscript. M.K. designed and performed experiments, analyzed data and wrote the
303 manuscript. C.F. designed and performed some experiments and analyzed some of the data.
304 M. Lavina provided technical help. O.D. participated in the supervision of the study, data
305 analysis and writing & editing of the manuscript.

306

307 **Declaration of interests**

308 The authors declare that there is no competing financial interest in this study.

309 **Figure 1. *Ex vivo* intestinal organoid model of *Listeria* infection**

310 (A) Experimental scheme and example of *Listeria* microinjection (details in the Methods). (B)
311 Example images of *Listeria* translocation (optical section). *LM* within a goblet cell, fixed 1
312 hour post microinjection (left panel; goblet cell marked with an arrow). *LM* basolaterally
313 extracellular beneath a goblet cell (right panel; goblet cells are marked with arrows). See also
314 Video S1. Translocated bacteria were distinguished from the total bacteria by consecutive
315 immunostaining, first against *LM* without permeabilization followed by tissue
316 permeabilization and labeling (Method). Scale bars, 10 μm (C) Quantification of *Listeria*
317 translocation. Top: Number of cells associated with bacteria either intracellularly or
318 basolaterally extracellularly per organoid. Bottom: Number of translocated bacteria per
319 organoid. Counts were performed in 12 organoids for each condition. Two-Way ANOVA test.
320 NS: Not significant; *****: $p < 0.0001$. See also Figure S1D,E, Video S1. (D) Light sheet live
321 imaging at indicated time point (top, maximum intensity projection (MIP); bottom, optical
322 section). Within 12 minutes, bacteria-containing vesicle reaches the basolateral side of the
323 cells, then exit from the cell in the following time points. Intracellular *Listeria* is surrounded
324 with membrane tomato (arrow). See also Video S2. (E) Left: Scheme depicting detection of
325 lumenally accessible Ecad from side and top view. Organoids were fixed, embedded,
326 sectioned to open the lumen and immunolabeled from the luminal side without
327 permeabilization. Ecad in the sectioned plane is exposed, thus accessible without
328 permeabilization and stained throughout the cutting plane (marked with green on the
329 drawing). Right: 3D-view of opened organoids from the side (top left) and top (bottom left).
330 Enlargement of boxed area on the left 3D-reconstructed organoids containing goblet cells
331 expressing lumenally accessible Ecad (center & right). Mucus that has been expelled is
332 marked with WGA conjugated with fluorophore. Accessible Ecad surrounds the expelled
333 mucus. Scale bars, 10 μm . See also Video S3. (F) Left: Scheme depicting detection Ecad
334 from side and top view. Organoids were fixed, embedded, sectioned to open the lumen,
335 permeabilized and immunolabeled from the luminal side. Total Ecad is stained (marked with
336 green on the drawing). Right: 3D-view of opened organoids from the side (top left) and top
337 (bottom left). Enlargement of boxed area on the left 3D-reconstructed organoids containing
338 goblet cell (center & right). Scale bars, 10 μm . See also Video S3.

339 **Figure 2. Endocytosis and microtubule dynamics are required for bacterial**
340 **translocation**

341 (A) Top: Experimental scheme of microinjection. Bottom: Confocal imaging of
342 permeabilized, whole-mount stained organoids treated with indicated inhibitors. In
343 cholchicine treated organoids, epithelium displayed more metaphase-blocked cells (+,
344 enlarged), indicating that cholchicine treatment worked (B) Quantification of number of cells
345 associated with bacteria. (C) Quantification of number of bacteria per organoid in indicated
346 location. Experiments were repeated 2 to 3 times. The results combine all experiments. 27
347 WT & dynasore-treated organoids and 21 colchicine-treated organoids were counted. Kruskall
348 Wallis test. Comparison to WT. NS: Not significant; *: $p < 0.5$; **: $p < 0.01$; ****: $p < 0.0001$.
349 See Also Figure S3. (D) Accessible Ecad from the luminal side of the sectioned organoids
350 treated with indicated inhibitors. See also Figure S2, Video S4. (E) Confocal images of
351 bacteria trapped inside the goblet cells in each condition (optical section from 3D
352 reconstruction, goblet cells are marked with an arrow). Bacteria are located in apical and
353 central side within the cells in dynasore- and cholchicine-treated conditions, respectively.
354 Bacteria are surrounded with a tomato-stained membrane. See also Figure S3 and Video S4.

355 **Figure 3. Inducible organoids expressing dominant-negative Rab11 and Rab7**
356 (A) Scheme depicting the organoid transduction. (B) Visualization of successful induction
357 with Dox for 16 hours. mCerulean (mCer) expression was detected by eyes using Zeiss Filter
358 set 38 HE (excitation BP 470/40, beamsplitter FT 495, emission BP 525/50). (C) Confocal
359 imaging of permeabilized, whole-mount stained organoids induced with indicated DN
360 proteins for 16 hours with Dox. Expression of DN proteins is visualized by anti-Rab7
361 (Rab7DN) or anti-myc (Rab11DN) staining. In mycRab11DN-induced organoids, mCer co-
362 localized with myc staining (not shown). Goblet cell producing mucus are labeled with WGA
363 (arrow). Junctional integrity of organoids is evaluated by Ecad staining.

364 **Figure 4. *Listeria* translocation requires functional Rab11 but not Rab7**

365 (A) Experimental scheme of microinjection. The organoids were grown in presence of
366 antibiotics (penicillin-streptomycin, geneticin and puromycin) and doxycycline was added 12-
367 16 hours before the microinjection. Induction of mCer was detected by eyes with Zeiss Filter
368 set 38 HE (excitation BP 470/40, beamsplitter FT 495, emission BP 525/50, Figure 3B).
369 Induced organoids were selected and microinjected, incubated for 2 hours (DN proteins still
370 being induced) followed by fixation & imaging. (B) Luminally accessible Ecad of the
371 sectioned organoids induced with indicated DN proteins. Accessible Ecad staining in XY, XZ
372 and YZ planes from indicated goblet cells (arrow from the right 3D reconstruction, sectioned
373 plane facing up in the side view). See also Video S5. (C) Optical sections from 3D
374 reconstruction of microinjected organoids induced for indicated DN proteins. *Li*-GFP (InlA)
375 can be detected beneath the basolateral side of the goblet cells in transduced, but non-induced
376 control (top) and in Rab7DN-induced organoids (center), indicating that bacterial
377 translocation occurred. *Li*-GFP (InlA) is trapped at the basal pole of the goblet cell, embedded
378 in WGA⁺ material in mycRab11DN-induced organoids (bottom). Goblet cells are marked
379 with an arrow. Scale bars, 20 μ m. See also Figure S3 and Video S5. (D) Quantification of
380 number of cells associated with bacteria per organoids. Kruskal Wallis test. Comparison to
381 WT. NI: Lentivirus transduced, non-induced control. NS: not significant. (E) Quantification
382 of number of bacteria per organoid in indicated location. Experiments were repeated 2 to 3
383 times. The results combine all experiments. Counts were performed in 19 non-induced, 18
384 Rab7DN and 24 Rab11DN organoids. The results for WT organoids are those from Figures
385 2B,C. Kruskal Wallis test. Comparison to WT. NS: Not significant; *: p<0.05; **: p<0.01.
386 See also Figure S3.

387 **STAR Methods**

388 **RESOURCES AVAILABILITY**

389

390 **Lead Contact**

391 Further information and requests for resources and reagents should be directed to and will be
392 fulfilled by the Lead Contact, Marc Lecuit (marc.lecuit@pasteur.fr).

393

394 **Materials Availability**

395 All plasmids generated in this study are available upon request.

396

397 **Data and Code Availability**

398 This study did not generate/analyze datasets or codes

399

400 **EXPERIMENTAL MODEL AND SUBJECT DETAILS**

401

402 **Bacteria**

403 For Figure 1B-C, *Lm* strain EGD (BUG 600) and isogenic deletion mutants $\Delta inlA$ (BUG 947
404 [56]), Δhly (BUG 2132 [57]), $\Delta actA$ (BUG 2140 [57]), *Li* WT (BUG 499), *Li*-expressing InlA
405 (*Li* (InlA+), BUG 1489 [23]) were used. We generated *Li*-expressing both InlA and GFP in
406 tandem under the phyper promoter of pAD vector, separated by the terminator sequence
407 (MBHL 366). Bacteria were transformed by electroporation. GFP expression was confirmed
408 by fluorescent microscopy, function of InlA was confirmed by *in vitro* invasion assay using
409 mouse fibroblast L2071 expressing human E-cadherin[49].

410

411 **Mice**

412 E16P KI mice were generated in the laboratory [16]. They were crossed with mT/mG mice
413 [59] to generate mtd-Tmt; E16P KI mice. Animal experiments were performed according to
414 the Institut Pasteur guidelines for laboratory animals' husbandry and in compliance with
415 European regulation 2010/63 EU. They were approved by the ethical committee
416 CETEA/CEEA No. 89 of Institut Pasteur under the number DHA180011.

417

418 **Organoids**

419 Intestinal organoids were generated and cultured from the crypts recovered from small
420 intestines of 6- to 8-week old KIE16P and mtd-Tmt; E16P KI mice using EDTA dissociation
421 method [9, 60]. They were grown in ENR medium (Advanced DMEM/F12 with EGF (50
422 ng/ml), Noggin (100 ng/ml) and R-spondin1 (500 ng/ml)).

423

424 **Cells**

425 HEK293T cells (ATCC CRL-11268) were grown and passaged in DMEM containing 2%
426 glutamine, 10% Tet-system approved FBS (Takara # 631106) and penicillin-streptomycin.

427

428 **METHOD DETAILS**

429

430 **Organoid microinjection**

431 Mature organoids growing in ENR medium were mechanically dissociated and passed into
432 the gridded, low-bottom iBidi-injection plate (Clinisciences # 80156). Result of Figure 1B-C
433 was obtained with ENR medium while all others were obtained using the following condition:
434 Organoids were passed in injection plates with 2:1 ratio of ENR and 50% of L-WRN cell-
435 conditioned media (made with Tet System Approved FBS, Takara # 631106) for 1-2 days to
436 have a round center to facilitate microinjection. When the organoids produced spherical
437 centers, the organoids were washed several times with pre-warmed Advanced DMEM/F12 to
438 remove the serum and excessive growth factors, replaced with either ENR or 5% L-WRN
439 conditioned media for minimal 1 day. A day before the microinjection, 10 μ M DAPT and 20
440 μ g/ml IL-13 were supplemented overnight to partially enrich the goblet cells and to induce
441 mucus expel from the existing goblet cells [61-63]. Figure 2A, final concentration of 80 μ M
442 dynasore or 10 μ g/ml colchicine were applied 2 hours prior to microinjection. Figure 4A & C,
443 final concentration of 2 μ g/ml doxycycline was added to the media 12-16 hours before the
444 microinjection. Microinjection was performed only to organoids verified to have successful
445 induction. Results of Figure 1B-C were obtained by fixing 1 hour and 16 hours, respectively,
446 after microinjection. The incubation period post microinjection of the other experiments was
447 optimized to 2 hours followed by fixation to reduce the damage of the organoids.
448 Drug/doxycycline treatment was maintained during this period. For live imaging, immediately
449 after microinjection, organoids were re-sampled to the imaging chamber of light sheet
450 microscope Zeiss Z1.

451 Overnight culture of bacteria was diluted (1/200) and grown until O.D 0.8, washed at least 3
452 times in PBS and collected as a final volume of 100 μ l in DMEM/F12 phenol red-free

453 medium. Microinjection was performed with Eppendorf InjectMan and FemtoJet system as
454 reported [64] using glass micropipettes injection needle (Vitromed # V-INJ-S3-35).

455

456 **Accessible Ecad detection**

457 Organoids were passed on the 8-well Lab-Tek plates and supplied with the media as for the
458 microinjection: first with 2:1 ratio of ENR and 50% L-WRN cell conditioned media to grow
459 the spherical center, followed by washing and either returned to ENR media or supplied with
460 5% L-WRN media for at least 1 day. A day before the fixation, organoids were treated at a
461 final concentration of 10 μ M DAPT and 20 ng/ml IL-13 overnight to induce mucus expel
462 from the existing goblet cells. Organoids were fixed with 4% PFA at 4°C overnight. For the
463 experiments in Figure 2D, final concentration of 80 μ M dynasore or 10 μ g/ml colchicine were
464 added 2 hours before fixation. Experiment of Figure 4B, final concentration of 2 μ g/ml
465 doxycycline was added 12-16 hours before fixation. When the organoids were fixed, PFA was
466 removed, organoids were washed and 6% low-melting agarose was poured to the wells.
467 Solidified wells were recovered, sectioned in 150-200 μ m thickness with a vibratome (Micro
468 HM 650V, Thermo Fisher Scientific). Sections containing opened organoids were blocked in
469 3% BSA in PBS and stained as indicated below.

470

471 **Immunofluorescence**

472 Accessible Ecad (Figure 1E, 2C and 4B): Organoids were fixed with 4% PFA at 4°C
473 overnight followed by washing and blocking with 3% BSA in PBS, overnight at room
474 temperature. Primary and secondary antibodies were applied for 1 hour at room temperature.

475

476 Whole-mount staining: Organoids were fixed with 4% PFA for 30 min – 1 hour at room
477 temperature followed by washing, blocking/permeabilizing for 2 hours either in 5% goat
478 serum with 1% Triton X-100 or in 3% BSA with 1% Triton X-100 in PBS. Primary
479 antibodies were applied at 4°C overnight followed by washing and stained with secondary
480 antibodies for 2 hours at room temperature or 4°C overnight.

481

482 Distinguishing intracellular vs translocated bacteria (Figure 1B): Organoids were fixed with
483 4% PFA at 37°C for 1 hour, washed and blocked without triton for 2 hours at room
484 temperature. Rabbit antisera against *Listeria monocytogenes* (R11 [55]) was added for 2 hours
485 at room temperature, followed by washing and secondary antibody for 1 hour at room
486 temperature to stain extra-organoid bacteria. Then microinjected organoids were

487 permeabilized with 1% Triton X-100 and stained with primary antibody at 4 °C overnight
488 followed by washing and secondary antibody for 2 hours at room temperature.

489
490 The following antibodies were used: anti-Ecad (Ecc2, Takara #M108, 1:350), anti-myc
491 (71D10, Cell Signaling # 2278, 1:500), anti-Rab7 (Sigma, #R4779, 1:200), WGA conjugated
492 with alexa 647 (Invitrogen, whole mount 1:300, section 1:1000) and Hoechst 33342
493 (Invitrogen 1:5000). Secondary antibodies include goat anti-rat conjugated with alexa 546,
494 goat anti-mouse conjugated with alexa 405, and goat anti-rabbit conjugated with alexa 405
495 (all Invitrogen 1:500). To identify the goblet cells, the following criteria were used, as the
496 Muc2 labeling method following Carnoy fixation and paraffin embedding [65] is not
497 compatible with our system, rendering the matrigel opaque as well as breaking the plate:
498 WGA⁺, typical goblet-shaped cellular morphology including the opening of the apical area
499 and the nucleus misaligned with neighboring cells. If the cells meet 2 or more conditions, we
500 regarded them as goblet cells.

501

502 **Imaging**

503 Images were acquired either by confocal microscope (fixed image, upright Zeiss LSM 700
504 equipped with a water Plan-Apochromat 40x/1.0 DIC M27 objective & inverted Zeiss LSM
505 710 equipped with an oil Plan-Apochromat 40x/1.3 DIC M27 objective) or light sheet
506 microscope (live image, Zeiss Z.1 equipped with a water Plan-Apochromat 40x/1.0 DIC
507 objective). For live imaging, imaging chamber was maintained at 37°C temperature, 5% CO₂
508 and supplemented with ENR media made with phenol red-free DMEM/F12. Three-dimension
509 reconstruction was performed using Arivis Vision 4D. 3.0.1 software. For Figure 1D and
510 video S2, the image was denoised using median filter (radius 1) followed by background
511 correction.

512

513 **Rab11DN and Rab7DN vector construction**

514 Rab11DN and Rab7DN were generated by mutagenesis PCR from the pCMV-intron myc
515 Rab11WT (Addgene #46785) and pCMV-SPORT6-Rab7, respectively.

516 Primers used for Rab11DN are: 5'-GTGTTGGAAAGAACAACCTCCTGTCTCGATTTA-3'
517 & 5'-GACAGGAGGTTGTTCTTTCCAACACCAGAATC-3'. Primers used for Rab7DN
518 are: 5'- CTGGTGTGGAAAGAACTCTCTCATGAACCAG -3' & 5'-
519 CTGGTTCATGAGAGAGTTCTTTCCAACACCAG -3'. DN constructs were cloned into the
520 multiple cloning site I (MCSI) and mCerulean sequence was cloned into the MCS II of Tet-

521 On® 3G Inducible Expression System (Bicistronic Version, pTRE3G-IRES, Takara #
522 631166)

523

524 **Lentivirus production and concentration**

525 Lentivirus particle containing tet-activator was purchased from Takara (#631311). Lentivirus
526 containing inducible mycRab11DN-mCer and Rab7DN-mCer constructs were produced using
527 calcium phosphate transfection in HEK293T cells (Takara # 631312, user protocol). 2nd
528 generation lentiviral plasmids psPAX2 and pMD2.G were used (Addgene #12260, #12259).
529 Lentivirus was concentrated with PEG-itTM (System Bioscience, # LV810A-1, user protocol).

530

531 **Organoid transduction**

532 Organoids were transduced with lentivirus using the method modified from Maru *et al.*, 2016
533 and Van Lidth de Jeude *et al.*, 2015 [11, 12]. Briefly, 1st generation of organoids from the
534 crypts were passed with ENR medium containing Wnt3a, CHIR99021 and Nicotinamide to
535 enrich stem cell population. 2-3 days later when the organoids display spheroid morphology
536 with few dead cells in the lumen, organoids were mechanically broken down and trypsinized
537 to single cells. Cells were washed and supplemented with the Lentivirus concentrate in a final
538 concentration of 1X ENR media containing Wnt 3a, CHIR99021, Nicotinamide,
539 TransDuxMAXTM with enhancer. Cells and virus mixture were incubated at 37°C water bath
540 for around 1 hour, distributed to a matrigel-coated 24 well plates, incubated in the 37°C
541 incubator for overnight. The next day, as live cells settle on the coated matrigel, supernatant
542 containing virus and dead cell debris was carefully removed and fresh matrigel was added to
543 form a sandwich having the live cells in the center of the two layers of the matrigel. ENR
544 medium containing Wnt3a, CHIR99021 and Nicotinamide (without TransDuxMAXTM) was
545 supplied for 2 more days. A final concentration of 1 µg/ml puromycin and 100 µg/ml
546 geneticin (neomycin) were added to select for the successful transduction with pTRE3G-DN
547 mutant-IRES;mCerulean and tet-activator, respectively, until the transduced stem cells form
548 small visible organoids. Media was returned to regular ENR media containing three
549 antibiotics (pen-strep, puromycin and geneticin) and transduced organoids were cultured in
550 presence of the three antibiotics throughout.

551

552 **QUANTIFICATION AND STATISTICAL ANALYSIS**

553

554 **Statistical Analysis**

555 All statistical analysis has been performed using Prism 8 (Graphpad). Details for statistical
556 tests used can be found in figure legends, including the number of replicates performed and
557 number of organoids analyzed for each condition and p-value

558

559 **Video legends**

560 **Video S1. *Listeria* crossing through intestinal organoid goblet cells. Related to Figure 1B**
561 **and Figure S1D.** 3D reconstruction of an intraluminally microinjected organoid, fixed 1 hour
562 post injection. *Li* (time 00:00-00:15: green, endogenous GFP thus intracellular; time 00:16-
563 00:25: cyan, double-labelled, thus translocated, see methods), Ecad (white) and WGA (red)
564 are indicated. 3D reconstruction (time 00:26-00:43, time 01:12-01:25) and optical section
565 (time 00:44-01:11) of *Li*-GFP (InIA) intraluminally microinjected organoids, expressing
566 membrane tomato and fixed 2 hours post injection. WGA (white) and nucleus (blue) are
567 indicated.

568

569 **Video S2. Real-time imaging of *Listeria* translocation. Related to Figure 1D.**

570 Intraluminally microinjected organoids expressing membrane tomato were imaged every 6
571 minutes for 2 hours. First and last horizontal rotation shows initial and last time point
572 (00:00:00 and 01:30:00), respectively. Bacterial translocation initiated between time point 8
573 and 9 (00:42:00 and 00:48:00) and ended between time point 15 and 16 (01:24:00 and
574 01:30:00). The white arrow indicates the bacterium being transcytosed.

575

576 **Video S3. Mucus-expelling goblet cells express lumenally accessible Ecad. Related to**
577 **Figure 1E, F.** Organoids were fixed, embedded in the agar, sectioned, immunolabeled from
578 the lumen without permeabilization (time 00:00-00:12) and with permeabilization (time
579 00:13-00:25). Ecad (green), WGA (red) and nucleus (blue) are indicated. Note that Ecad in
580 the sectioned plane is exposed, thus accessible without permeabilization and stained
581 throughout the cut plane. Goblet cell enlarged in Figure 1E is marked with an arrow.

582

583 **Video S4. *Listeria* translocation is impaired when Ecad endocytosis and microtubule**
584 **dynamics are inhibited. Related to Figure 2D, E.** Lumenally accessible Ecad in mucus-
585 expelling goblet cells in dynasore-treated organoids (time 00:00-00:12) and in cholchicine-
586 treated organoids (time 00:13-00:24). Apical intracellular *Listeria* in dynasore-treated
587 organoid (time 00:25-00:36) and *Listeria* in the central part inside the goblet cell in
588 cholchicine-treated organoids (time 00:37-00:48).

589

590 **Video S5. *Listeria* translocation is impaired in Rab11DN but not in Rab7DN-induced**
591 **organoids. Related to Figure 4B, C.** Lumenally accessible Ecad in mucus-expelling goblet
592 cells in Rab7DN-induced organoids (time 00:00-00:12) and in Rab11DN-induced organoids

593 (time 00:13-00:24). *Listeria* translocated across the goblet cells in Rab7DN-induced organoid
594 (time 00:25-00:44) and *Listeria* trapped in the basolateral pole of goblet cell in Rab11DN-
595 induced organoids (time 00:45-01:01). *Listeria* trapped in mucus inside the goblet cell is
596 indicated by an arrow.
597 .

References

- 600 1. Lecuit, M. (2020). *Listeria monocytogenes*, a model in infection biology. *Cell*
601 *Microbiol* 22, e13186.
- 602 2. Gaillard, J.L., Berche, P., Frehel, C., Gouin, E., and Cossart, P. (1991). Entry of *L.*
603 *monocytogenes* into cells is mediated by internalin, a repeat protein reminiscent of
604 surface antigens from gram-positive cocci. *Cell* 65, 1127-1141.
- 605 3. Mengaud, J., Ohayon, H., Gounon, P., Mege, R.M., and Cossart, P. (1996). E-cadherin
606 is the receptor for internalin, a surface protein required for entry of *L. monocytogenes*
607 into epithelial cells. *Cell* 84, 923-932.
- 608 4. Lecuit, M., Dramsi, S., Gottardi, C., Fedor-Chaiken, M., Gumbiner, B., and Cossart,
609 P. (1999). A single amino acid in E-cadherin responsible for host specificity towards
610 the human pathogen *Listeria monocytogenes*. *EMBO J* 18, 3956-3963.
- 611 5. Lecuit, M., Vandormael-Pournin, S., Lefort, J., Huerre, M., Gounon, P., Dupuy, C.,
612 Babinet, C., and Cossart, P. (2001). A transgenic model for listeriosis: role of
613 internalin in crossing the intestinal barrier. *Science* 292, 1722-1725.
- 614 6. Nikitas, G., Deschamps, C., Disson, O., Niault, T., Cossart, P., and Lecuit, M. (2011).
615 Transcytosis of *Listeria monocytogenes* across the intestinal barrier upon specific
616 targeting of goblet cell accessible E-cadherin. *J Exp Med* 208, 2263-2277.
- 617 7. Le, T.L., Yap, A.S., and Stow, J.L. (1999). Recycling of E-cadherin: a potential
618 mechanism for regulating cadherin dynamics. *J Cell Biol* 146, 219-232.
- 619 8. Bruser, L., and Bogdan, S. (2017). Adherens Junctions on the Move-Membrane
620 Trafficking of E-Cadherin. *Cold Spring Harb Perspect Biol* 9.
- 621 9. Sato, T., Vries, R.G., Snippert, H.J., van de Wetering, M., Barker, N., Stange, D.E.,
622 van Es, J.H., Abo, A., Kujala, P., Peters, P.J., et al. (2009). Single Lgr5 stem cells
623 build crypt-villus structures in vitro without a mesenchymal niche. *Nature* 459, 262-
624 265.
- 625 10. Koo, B.K., Stange, D.E., Sato, T., Karthaus, W., Farin, H.F., Huch, M., van Es, J.H.,
626 and Clevers, H. (2011). Controlled gene expression in primary Lgr5 organoid cultures.
627 *Nat Methods* 9, 81-83.
- 628 11. Maru, Y., Orihashi, K., and Hippo, Y. (2016). Lentivirus-Based Stable Gene Delivery
629 into Intestinal Organoids. *Methods Mol Biol* 1422, 13-21.
- 630 12. Van Lidth de Jeude, J.F., Vermeulen, J.L., Montenegro-Miranda, P.S., Van den Brink,
631 G.R., and Heijmans, J. (2015). A protocol for lentiviral transduction and downstream
632 analysis of intestinal organoids. *J Vis Exp*.
- 633 13. Schwank, G., and Clevers, H. (2016). CRISPR/Cas9-Mediated Genome Editing of
634 Mouse Small Intestinal Organoids. *Methods Mol Biol* 1422, 3-11.
- 635 14. Yin, X., Farin, H.F., van Es, J.H., Clevers, H., Langer, R., and Karp, J.M. (2014).
636 Niche-independent high-purity cultures of Lgr5+ intestinal stem cells and their
637 progeny. *Nat Methods* 11, 106-112.
- 638 15. McKinley, K.L., Stuurman, N., Royer, L.A., Schartner, C., Castillo-Azofeifa, D.,
639 Delling, M., Klein, O.D., and Vale, R.D. (2018). Cellular aspect ratio and cell division
640 mechanics underlie the patterning of cell progeny in diverse mammalian epithelia.
641 *Elife* 7.
- 642 16. Disson, O., Grayo, S., Huillet, E., Nikitas, G., Langa-Vives, F., Dussurget, O., Ragon,
643 M., Le Monnier, A., Babinet, C., Cossart, P., et al. (2008). Conjugated action of two
644 species-specific invasion proteins for fetoplacental listeriosis. *Nature* 455, 1114-1118.
- 645 17. de Lau, W., Kujala, P., Schneeberger, K., Middendorp, S., Li, V.S., Barker, N.,
646 Martens, A., Hofhuis, F., DeKoter, R.P., Peters, P.J., et al. (2012). Peyer's patch M

- 647 cells derived from Lgr5(+) stem cells require SpiB and are induced by RankL in
648 cultured "miniguts". *Mol Cell Biol* 32, 3639-3647.
- 649 18. Colony, P.C. (1996). Structural characterization of colonic cell types and correlation
650 with specific functions. *Dig Dis Sci* 41, 88-104.
- 651 19. Johansson, M.E., and Hansson, G.C. (2012). Preservation of mucus in histological
652 sections, immunostaining of mucins in fixed tissue, and localization of bacteria with
653 FISH. *Methods Mol Biol* 842, 229-235.
- 654 20. Fischer, J., Uhlenbruck, G., Klein, P.J., Vierbuchen, M., and Fischer, R. (1984).
655 Characterization of glycoconjugates of human gastrointestinal mucosa by lectins. II.
656 Lectin binding to the isolated glycoproteins of normal and malignant gastric mucosa. *J*
657 *Histochem Cytochem* 32, 690-696.
- 658 21. Fischer, J., Klein, P.J., Vierbuchen, M., Skutta, B., Uhlenbruck, G., and Fischer, R.
659 (1984). Characterization of glycoconjugates of human gastrointestinal mucosa by
660 lectins. I. Histochemical distribution of lectin binding sites in normal alimentary tract
661 as well as in benign and malignant gastric neoplasms. *J Histochem Cytochem* 32, 681-
662 689.
- 663 22. Knoop, K.A., McDonald, K.G., McCrate, S., McDole, J.R., and Newberry, R.D.
664 (2015). Microbial sensing by goblet cells controls immune surveillance of luminal
665 antigens in the colon. *Mucosal Immunol* 8, 198-210.
- 666 23. Lecuit, M., Ohayon, H., Braun, L., Mengaud, J., and Cossart, P. (1997). Internalin of
667 *Listeria monocytogenes* with an intact leucine-rich repeat region is sufficient to
668 promote internalization. *Infect Immun* 65, 5309-5319.
- 669 24. Coelho, C., Brown, L., Maryam, M., Vij, R., Smith, D.F.Q., Burnet, M.C., Kyle, J.E.,
670 Heyman, H.M., Ramirez, J., Prados-Rosales, R., et al. (2019). *Listeria monocytogenes*
671 virulence factors, including listeriolysin O, are secreted in biologically active
672 extracellular vesicles. *J Biol Chem* 294, 1202-1217.
- 673 25. Hunt, S.D., Townley, A.K., Danson, C.M., Cullen, P.J., and Stephens, D.J. (2013).
674 Microtubule motors mediate endosomal sorting by maintaining functional domain
675 organization. *J Cell Sci* 126, 2493-2501.
- 676 26. Desclozeaux, M., Venturato, J., Wylie, F.G., Kay, J.G., Joseph, S.R., Le, H.T., and
677 Stow, J.L. (2008). Active Rab11 and functional recycling endosome are required for
678 E-cadherin trafficking and lumen formation during epithelial morphogenesis.
679 *American Journal of Physiology-Cell Physiology* 295, C545-C556.
- 680 27. Langevin, J., Morgan, M.J., Rosse, C., Racine, V., Sibarita, J.B., Aresta, S., Murthy,
681 M., Schwarz, T., Camonis, J., and Bellaiche, Y. (2005). *Drosophila* exocyst
682 components Sec5, Sec6, and Sec15 regulate DE-cadherin trafficking from recycling
683 endosomes to the plasma membrane. *Developmental Cell* 9, 365-376.
- 684 28. Palacios, F., Schweitzer, J.K., Boshans, R.L., and D'Souza-Schorey, C. (2002). ARF6-
685 GTP recruits Nm23-H1 to facilitate dynamin-mediated endocytosis during adherens
686 junctions disassembly. *Nat Cell Biol* 4, 929-936.
- 687 29. de Beco, S., Guedry, C., Amblard, F., and Coscoy, S. (2009). Endocytosis is required
688 for E-cadherin redistribution at mature adherens junctions. *Proc Natl Acad Sci U S A*
689 *106*, 7010-7015.
- 690 30. Delevoe, C., Miserey-Lenkei, S., Montagnac, G., Gilles-Marsens, F., Paul-
691 Gilloteaux, P., Giordano, F., Waharte, F., Marks, M.S., Goud, B., and Raposo, G.
692 (2014). Recycling endosome tubule morphogenesis from sorting endosomes requires
693 the kinesin motor KIF13A. *Cell Rep* 6, 445-454.
- 694 31. Meng, W., Mushika, Y., Ichii, T., and Takeichi, M. (2008). Anchorage of microtubule
695 minus ends to adherens junctions regulates epithelial cell-cell contacts. *Cell* 135, 948-
696 959.

- 697 32. Veiga, E., Guttman, J.A., Bonazzi, M., Boucrot, E., Toledo-Arana, A., Lin, A.E.,
698 Enninga, J., Pizarro-Cerda, J., Finlay, B.B., Kirchhausen, T., et al. (2007). Invasive
699 and adherent bacterial pathogens co-Opt host clathrin for infection. *Cell Host Microbe*
700 *2*, 340-351.
- 701 33. Macia, E., Ehrlich, M., Massol, R., Boucrot, E., Brunner, C., and Kirchhausen, T.
702 (2006). Dynasore, a cell-permeable inhibitor of dynamin. *Dev Cell* *10*, 839-850.
- 703 34. Taylor, E.W. (1965). The Mechanism of Colchicine Inhibition of Mitosis. I. Kinetics
704 of Inhibition and the Binding of H3-Colchicine. *J Cell Biol* *25*, SUPPL:145-160.
- 705 35. Kessell, I., Holst, B.D., and Roth, T.F. (1989). Membranous intermediates in
706 endocytosis are labile, as shown in a temperature-sensitive mutant. *Proc Natl Acad Sci*
707 *U S A* *86*, 4968-4972.
- 708 36. Damke, H., Baba, T., Warnock, D.E., and Schmid, S.L. (1994). Induction of mutant
709 dynamin specifically blocks endocytic coated vesicle formation. *J Cell Biol* *127*, 915-
710 934.
- 711 37. Henley, J.R., Krueger, E.W., Oswald, B.J., and McNiven, M.A. (1998). Dynamin-
712 mediated internalization of caveolae. *J Cell Biol* *141*, 85-99.
- 713 38. Lock, J.G., and Stow, J.L. (2005). Rab11 in recycling endosomes regulates the sorting
714 and basolateral transport of E-cadherin. *Molecular Biology of the Cell* *16*, 1744-1755.
- 715 39. Woichansky, I., Beretta, C.A., Berns, N., and Riechmann, V. (2016). Three
716 mechanisms control E-cadherin localization to the zonula adherens. *Nat Commun* *7*,
717 10834.
- 718 40. Sonnichsen, B., De Renzis, S., Nielsen, E., Rietdorf, J., and Zerial, M. (2000). Distinct
719 membrane domains on endosomes in the recycling pathway visualized by multicolor
720 imaging of Rab4, Rab5, and Rab11. *J Cell Biol* *149*, 901-914.
- 721 41. Ullrich, O., Reinsch, S., Urbe, S., Zerial, M., and Parton, R.G. (1996). Rab11 regulates
722 recycling through the pericentriolar recycling endosome. *J Cell Biol* *135*, 913-924.
- 723 42. Yu, S., Yehia, G., Wang, J., Stypulkowski, E., Sakamori, R., Jiang, P., Hernandez-
724 Enriquez, B., Tran, T.S., Bonder, E.M., Guo, W., et al. (2014). Global ablation of the
725 mouse Rab11a gene impairs early embryogenesis and matrix metalloproteinase
726 secretion. *J Biol Chem* *289*, 32030-32043.
- 727 43. Sobajima, T., Yoshimura, S., Iwano, T., Kunii, M., Watanabe, M., Atik, N., Mushiake,
728 S., Morii, E., Koyama, Y., Miyoshi, E., et al. (2014). Rab11a is required for apical
729 protein localisation in the intestine. *Biol Open* *4*, 86-94.
- 730 44. Palacios, F., Tushir, J.S., Fujita, Y., and D'Souza-Schorey, C. (2005). Lysosomal
731 targeting of E-cadherin: a unique mechanism for the down-regulation of cell-cell
732 adhesion during epithelial to mesenchymal transitions. *Mol Cell Biol* *25*, 389-402.
- 733 45. Ettayebi, K., Crawford, S.E., Murakami, K., Broughman, J.R., Karandikar, U., Tenge,
734 V.R., Neill, F.H., Blutt, S.E., Zeng, X.L., Qu, L., et al. (2016). Replication of human
735 noroviruses in stem cell-derived human enteroids. *Science* *353*, 1387-1393.
- 736 46. Lamers, M.M., Beumer, J., van der Vaart, J., Knoops, K., Puschhof, J., Breugem, T.I.,
737 Ravelli, R.B.G., Paul van Schayck, J., Mykytyn, A.Z., Duimel, H.Q., et al. (2020).
738 SARS-CoV-2 productively infects human gut enterocytes. *Science*.
- 739 47. Forbester, J.L., Goulding, D., Vallier, L., Hannan, N., Hale, C., Pickard, D.,
740 Mukhopadhyay, S., and Dougan, G. (2015). Interaction of *Salmonella enterica*
741 Serovar Typhimurium with Intestinal Organoids Derived from Human Induced
742 Pluripotent Stem Cells. *Infect Immun* *83*, 2926-2934.
- 743 48. Heo, I., Dutta, D., Schaefer, D.A., Iakobachvili, N., Artegiani, B., Sachs, N.,
744 Boonekamp, K.E., Bowden, G., Hendrickx, A.P.A., Willems, R.J.L., et al. (2018).
745 Modelling *Cryptosporidium* infection in human small intestinal and lung organoids.
746 *Nat Microbiol* *3*, 814-823.

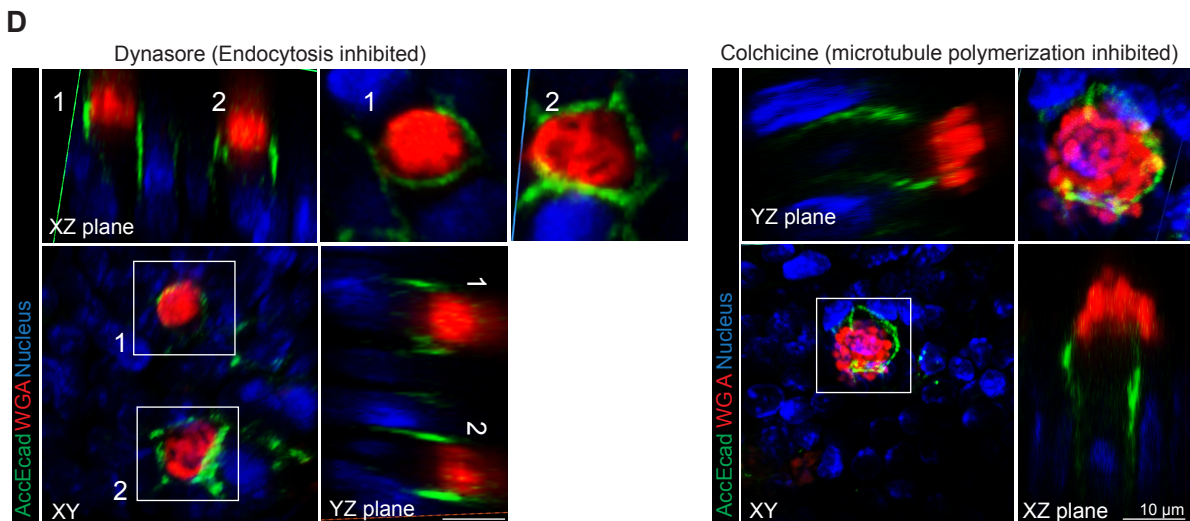
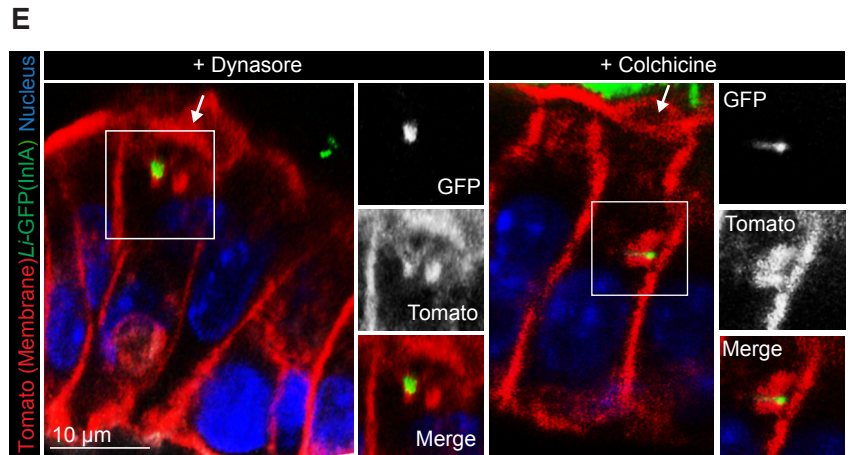
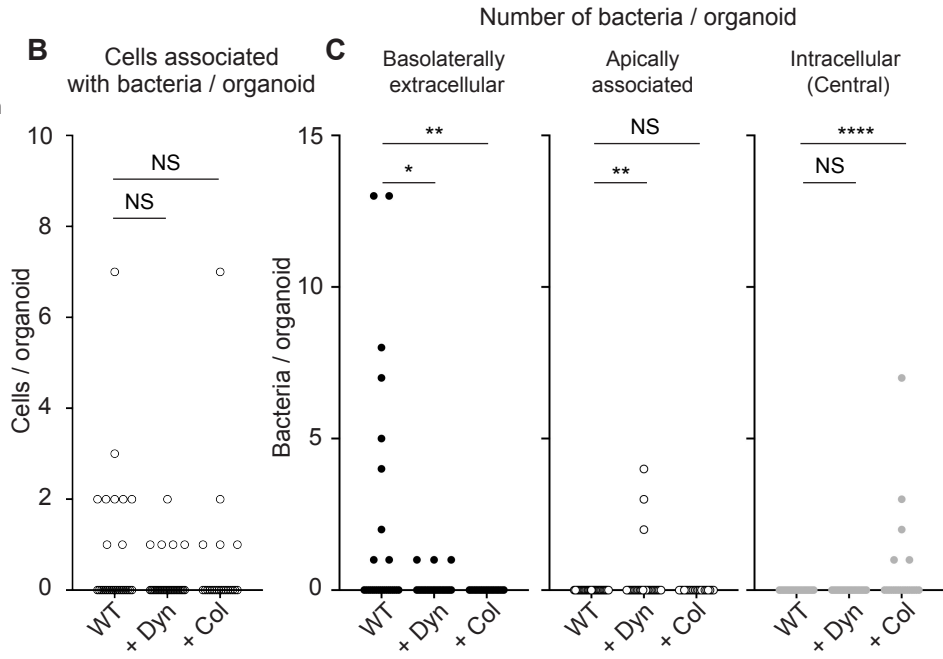
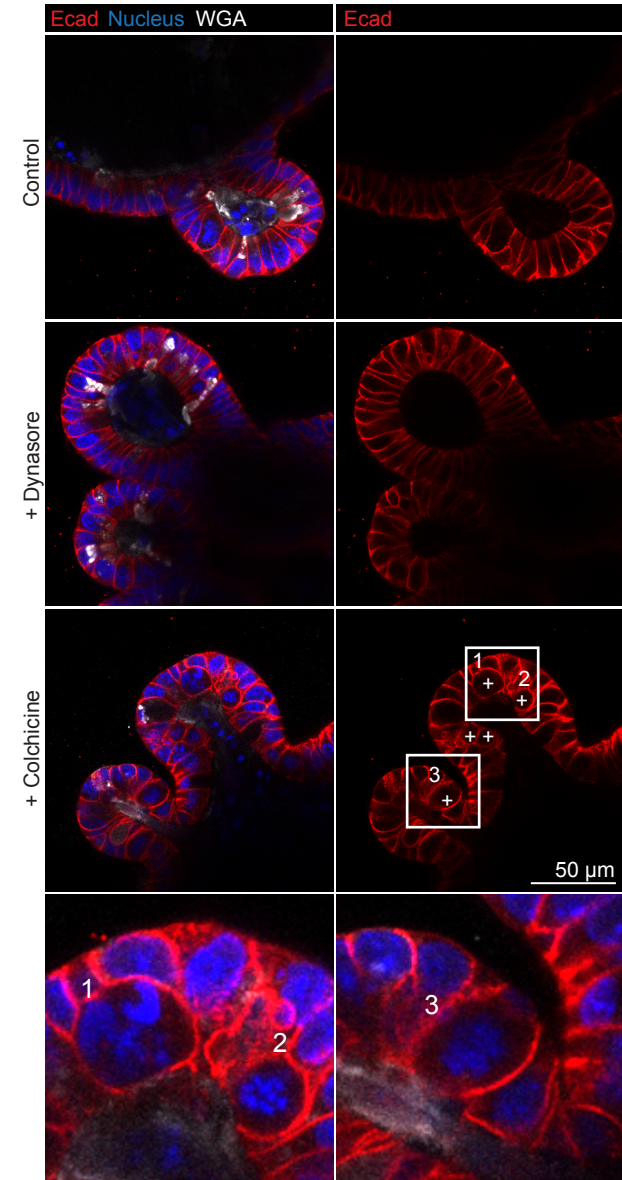
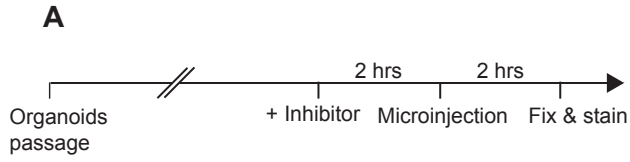
- 747 49. Lecuit, M., Hurme, R., Pizarro-Cerda, J., Ohayon, H., Geiger, B., and Cossart, P.
748 (2000). A role for alpha-and beta-catenins in bacterial uptake. *Proc Natl Acad Sci U S*
749 *A 97*, 10008-10013.
- 750 50. Bonazzi, M., Veiga, E., Pizarro-Cerda, J., and Cossart, P. (2008). Successive post-
751 translational modifications of E-cadherin are required for InlA-mediated
752 internalization of *Listeria monocytogenes*. *Cell Microbiol 10*, 2208-2222.
- 753 51. Sousa, S., Cabanes, D., El-Amraoui, A., Petit, C., Lecuit, M., and Cossart, P. (2004).
754 Unconventional myosin VIIa and vezatin, two proteins crucial for *Listeria* entry into
755 epithelial cells. *J Cell Sci 117*, 2121-2130.
- 756 52. Sousa, S., Cabanes, D., Bougneres, L., Lecuit, M., Sansonetti, P., Tran-Van-Nhieu, G.,
757 and Cossart, P. (2007). Src, cortactin and Arp2/3 complex are required for E-cadherin-
758 mediated internalization of *Listeria* into cells. *Cell Microbiol 9*, 2629-2643.
- 759 53. Sousa, S., Cabanes, D., Archambaud, C., Colland, F., Lemichez, E., Popoff, M.,
760 Boisson-Dupuis, S., Gouin, E., Lecuit, M., Legrain, P., et al. (2005). ARHGAP10 is
761 necessary for alpha-catenin recruitment at adherens junctions and for *Listeria* invasion.
762 *Nat Cell Biol 7*, 954-960.
- 763 54. Tilney, L.G., and Portnoy, D.A. (1989). Actin filaments and the growth, movement,
764 and spread of the intracellular bacterial parasite, *Listeria monocytogenes*. *J Cell Biol*
765 *109*, 1597-1608.
- 766 55. Dramsi, S., Levi, S., Triller, A., and Cossart, P. (1998). Entry of *Listeria*
767 *monocytogenes* into neurons occurs by cell-to-cell spread: an in vitro study. *Infect*
768 *Immun 66*, 4461-4468.
- 769 56. Dramsi, S., Biswas, I., Maguin, E., Braun, L., Mastroeni, P., and Cossart, P. (1995).
770 Entry of *Listeria monocytogenes* into hepatocytes requires expression of inlB, a
771 surface protein of the internalin multigene family. *Mol Microbiol 16*, 251-261.
- 772 57. Levraud, J.P., Disson, O., Kissa, K., Bonne, I., Cossart, P., Herbomel, P., and Lecuit,
773 M. (2009). Real-time observation of *Listeria monocytogenes*-phagocyte interactions in
774 living zebrafish larvae. *Infect Immun 77*, 3651-3660.
- 775 58. Balestrino, D., Hamon, M.A., Dortet, L., Nahori, M.A., Pizarro-Cerda, J., Alignani,
776 D., Dussurget, O., Cossart, P., and Toledo-Arana, A. (2010). Single-cell techniques
777 using chromosomally tagged fluorescent bacteria to study *Listeria monocytogenes*
778 infection processes. *Appl Environ Microbiol 76*, 3625-3636.
- 779 59. Muzumdar, M.D., Tasic, B., Miyamichi, K., Li, L., and Luo, L. (2007). A global
780 double-fluorescent Cre reporter mouse. *Genesis 45*, 593-605.
- 781 60. Mahe, M.M., Aihara, E., Schumacher, M.A., Zavros, Y., Montrose, M.H., Helmrath,
782 M.A., Sato, T., and Shroyer, N.F. (2013). Establishment of Gastrointestinal Epithelial
783 Organoids. *Curr Protoc Mouse Biol 3*, 217-240.
- 784 61. Waddell, A., Vallance, J.E., Hummel, A., Alenghat, T., and Rosen, M.J. (2019). IL-33
785 Induces Murine Intestinal Goblet Cell Differentiation Indirectly via Innate Lymphoid
786 Cell IL-13 Secretion. *J Immunol 202*, 598-607.
- 787 62. Wu, D., Ahrens, R., Osterfeld, H., Noah, T.K., Groschwitz, K., Foster, P.S.,
788 Steinbrecher, K.A., Rothenberg, M.E., Shroyer, N.F., Matthaei, K.I., et al. (2011).
789 Interleukin-13 (IL-13)/IL-13 receptor alpha1 (IL-13Ralpha1) signaling regulates
790 intestinal epithelial cystic fibrosis transmembrane conductance regulator channel-
791 dependent Cl⁻ secretion. *J Biol Chem 286*, 13357-13369.
- 792 63. van Es, J.H., van Gijn, M.E., Riccio, O., van den Born, M., Vooijs, M., Begthel, H.,
793 Cozijnsen, M., Robine, S., Winton, D.J., Radtke, F., et al. (2005). Notch/gamma-
794 secretase inhibition turns proliferative cells in intestinal crypts and adenomas into
795 goblet cells. *Nature 435*, 959-963.

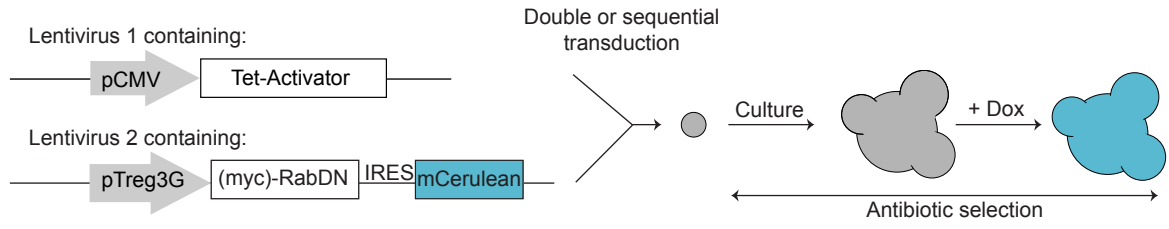
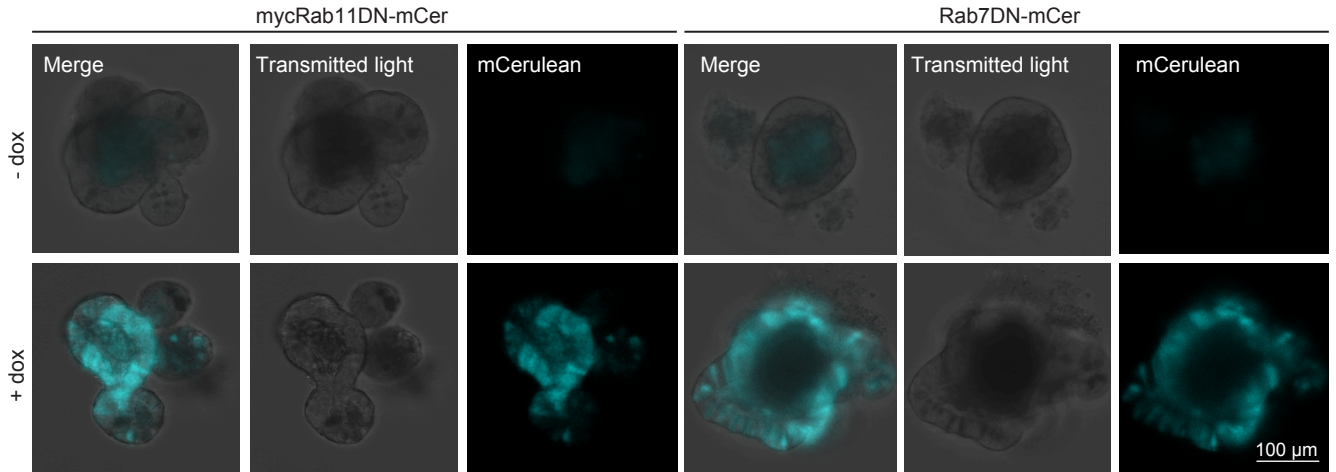
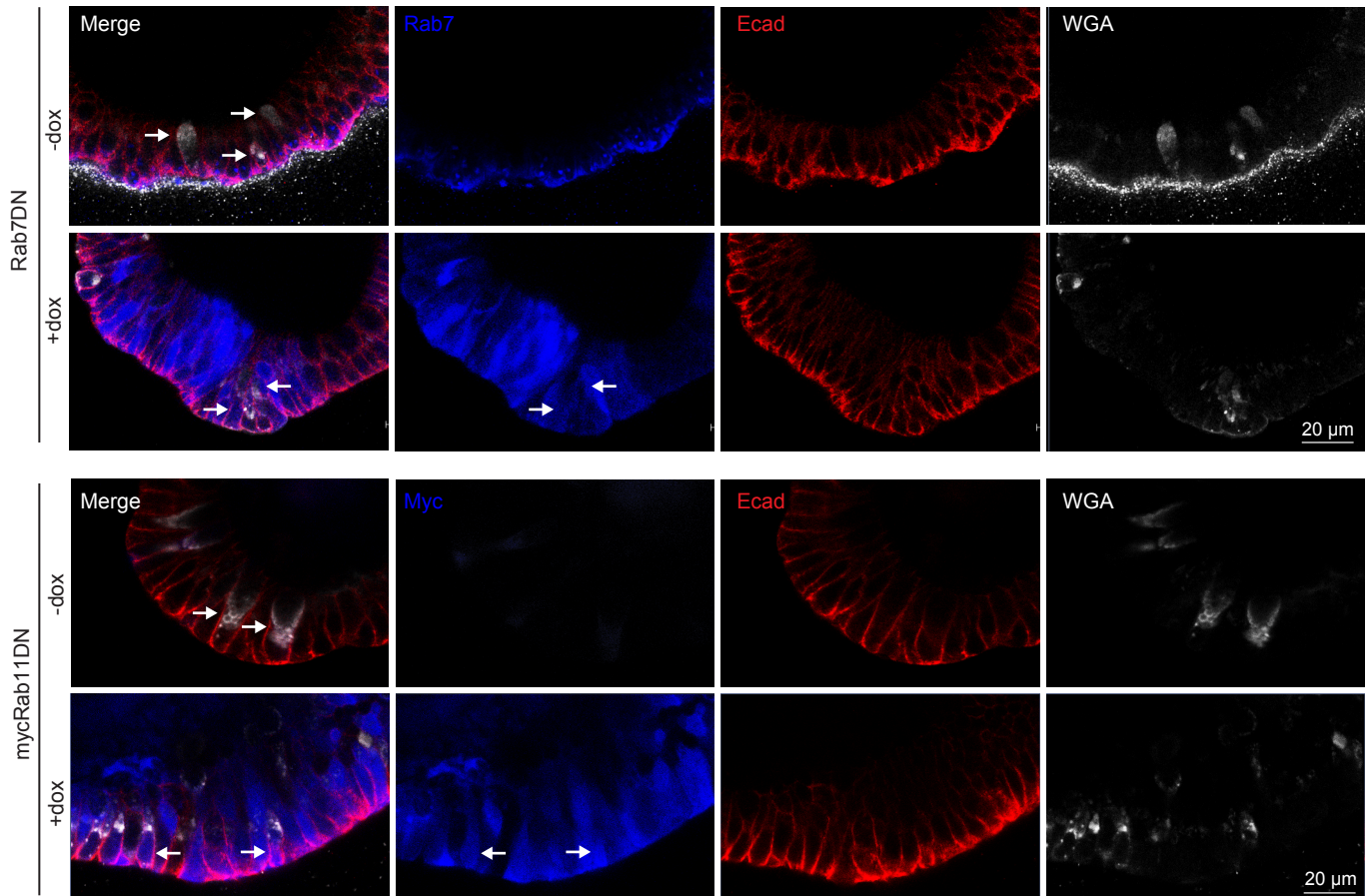
- 796 64. Nigro, G., Hanson, M., Fevre, C., Lecuit, M., and Sansonetti, P.J. (2019). Intestinal
797 Organoids as a Novel Tool to Study Microbes-Epithelium Interactions. *Methods Mol*
798 *Biol* *1576*, 183-194.
- 799 65. Johansson, M.E., Phillipson, M., Petersson, J., Velcich, A., Holm, L., and Hansson,
800 G.C. (2008). The inner of the two Muc2 mucin-dependent mucus layers in colon is
801 devoid of bacteria. *Proc Natl Acad Sci U S A* *105*, 15064-15069.
802

KEY RESOURCES TABLE

REAGENT or RESOURCE	SOURCE	IDENTIFIER
Antibodies and fluorescent dyes		
Rat anti-E-cad (Eccd2)	Takara	#M108
Rabbit anti Rab7	Sigma	R4779
Rabbit antisera against <i>Listeria monocytogenes</i>	[55]	R11
Mouse IgG1 anti-myc (71D10)	Cell signaling	#2278
WGA-conjugated with Alexa Fluor 647	Invitrogen	W32466
Hoechst 33342	Invitrogen	H3570
Goat anti-Rat Alexa Fluor 546	Invitrogen	#A-11081
Goat anti-Rabbit Alexa Fluor 405	Invitrogen	#A-31556
Goat anti-Mouse Alexa Fluor 405	Invitrogen	#A-31553
Bacterial and Virus Strains		
<i>Lm</i> strain EGD	[56]	BUG600
EGD Δ <i>inlA</i>	[56]	BUG 947
EGD Δ <i>hly</i>	[57]	BUG 2132
EGD Δ <i>actA</i>	[57]	BUG 2140
<i>Li</i> WT	[55]	BUG 499
<i>Li</i> (InlA+)	[23]	BUG 1489
<i>Li</i> -GFP (InlA+)	This paper	MBHL 366
rLV.EF1.Tet3G-9	Takara	631311
Chemicals, Peptides, and Recombinant Proteins		
N2 Supplement	Gibco Invitrogen	#17502048
B27 Supplement	Gibco Invitrogen	#17504044
N-Acetylcystein	Sigma Aldrich	#A9165-5G
Human recombinant R-spondin 1 (final 500 ng/ml)	R&D systems	#4645-RS250
Mouse recombinant Noggin (final 100 ng/ml)	Peprotech	#250-38-20ug
Mouse recombinant EGF (final 50 ng/ml)	Invitrogen	#PMG8044
Y-27632 (final 10 μ M)	Sigma Aldrich	#Y0503-1MG
Mouse recombinant Wnt3a (final 100 ng/ml)	Millipore	#GF160
Nicotinamide (final 10 mM)	Sigma Aldrich	#N0636-100g
CHIR99021 (final 10 μ M)	Stemgent	#248040004
Doxycycline (final 2 μ g/ml)	Takara	#631311
Dynasore (final 80 μ M)	Sigma	324410-10MG
Colchicine (final 10 μ g/ml)	Sigma	C3915
DATP (final 10 μ M)	Stemgent	#04-0041
IL-13 (final 20 ng/ml)	R&D systems	#413-ML-005
TransDux MAX TM	System Bioscience	LV860A-1
Matrigel	Corning	356231
Cell recovery solution	BD	354253
Advanced DMEM/F12	Gibco Invitrogen	12634010
DMEM/F12 phenol red-free	Gibco Invitrogen	21041025
GlutaMAX	Gibco Invitrogen	35050038
1M HEPES	Gibco Invitrogen	15630056
Penicillin-streptomycin	Gibco Invitrogen	15140163
Puromycin (final 1 μ g/ml)	Sigma	540411-25MG

Neomycin (Geneticin, final 1X)	Gibco Invitrogen	10138031
Critical Commercial Assays		
Calcium phosphate transfection kit	Takara	#631312
PEG-it TM Virus precipitation solution	System Bioscience	# LV810A-1
Experimental Models: Cell Lines		
HEK293T	ATCC	#CRL-11268
L-WRN	ATCC	#CRL-3276
Experimental Models: Organisms/Strains		
Mouse (KI E16P) intestinal organoid	This paper and [16]	N/A
Mouse (mtd-Tmt; KI E16P) intestinal organoid	This paper and [6]	N/A
Oligonucleotides		
Primer for Rab11DN 5'-GTGTTGGAAGAACAACCTCCTGTCTCGATTTA-3'	This paper	N/A
Primer for Rab11DN 5'-GACAGGAGGTTGTTCTTTCCAACACCAGAA TC-3'	This paper	N/A
Primer for Rab7DN 5'-CTGGTGTGGAAGA ACTCTCTCATGAACCA G -3'	This paper	N/A
Primer for Rab7DN 5'-CTGGTTCATGAGAGAGTTCTTTCCAACACCAG -3'	This paper	N/A
Recombinant DNA		
pAD	[58]	N/A
psPAX2	Addgene	#12260
pMD2.G	Addgene	#12259
pTREG3-IRES	Takara	#631312
pCMV-intron-mycRab11	Addgene	#46785
pCMV-SPORT6-Rab7	Addgene and this paper	N/A
Software and Algorithms		
Prism 8	Graphpad	
Arivis Vision4D 3.0.	Arivis	
FIJI	ImageJ	
ZEN 2014 SP1	ZEISS	



A**B****C**

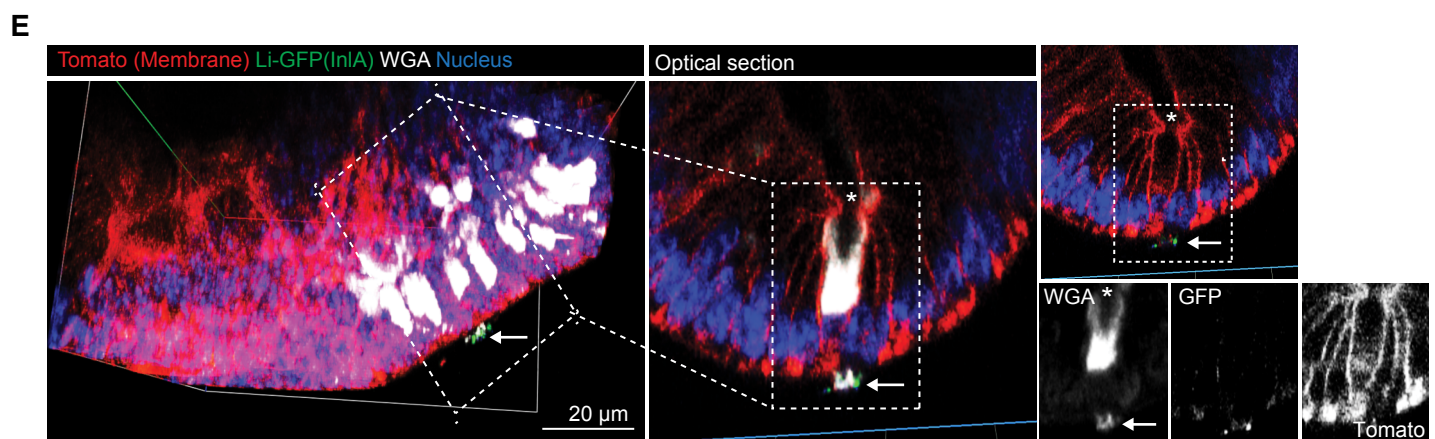
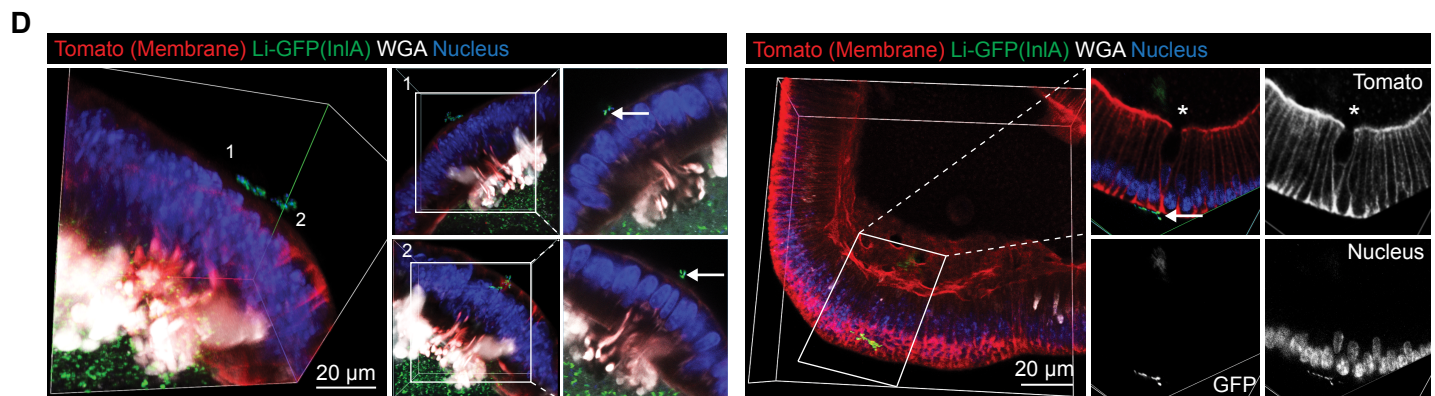
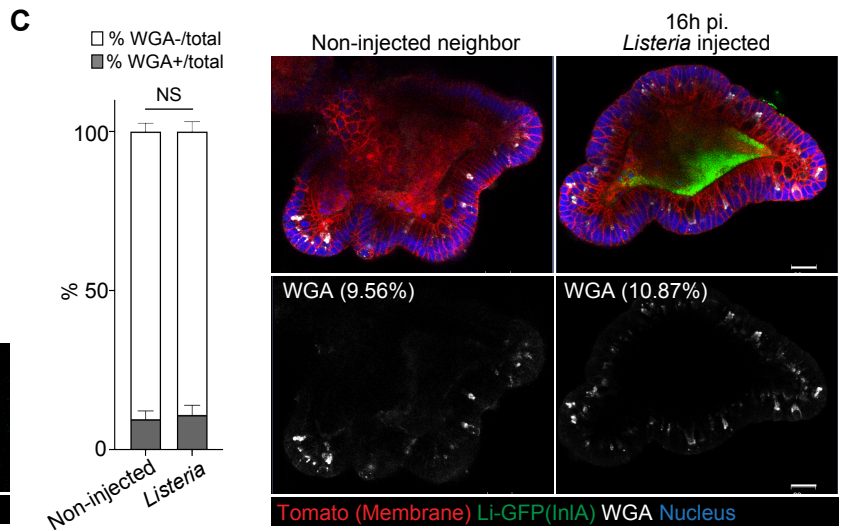
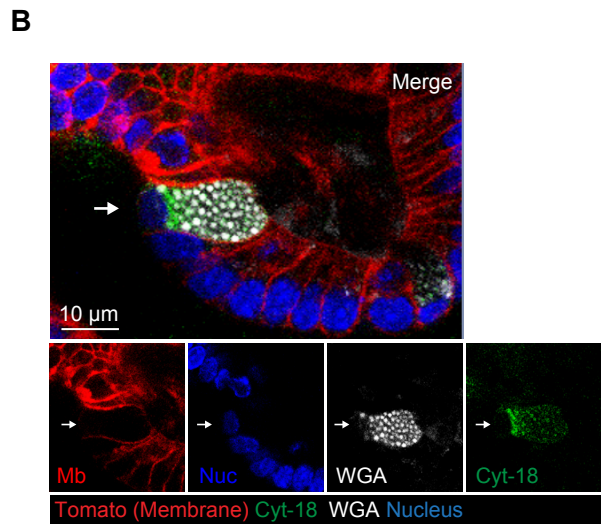
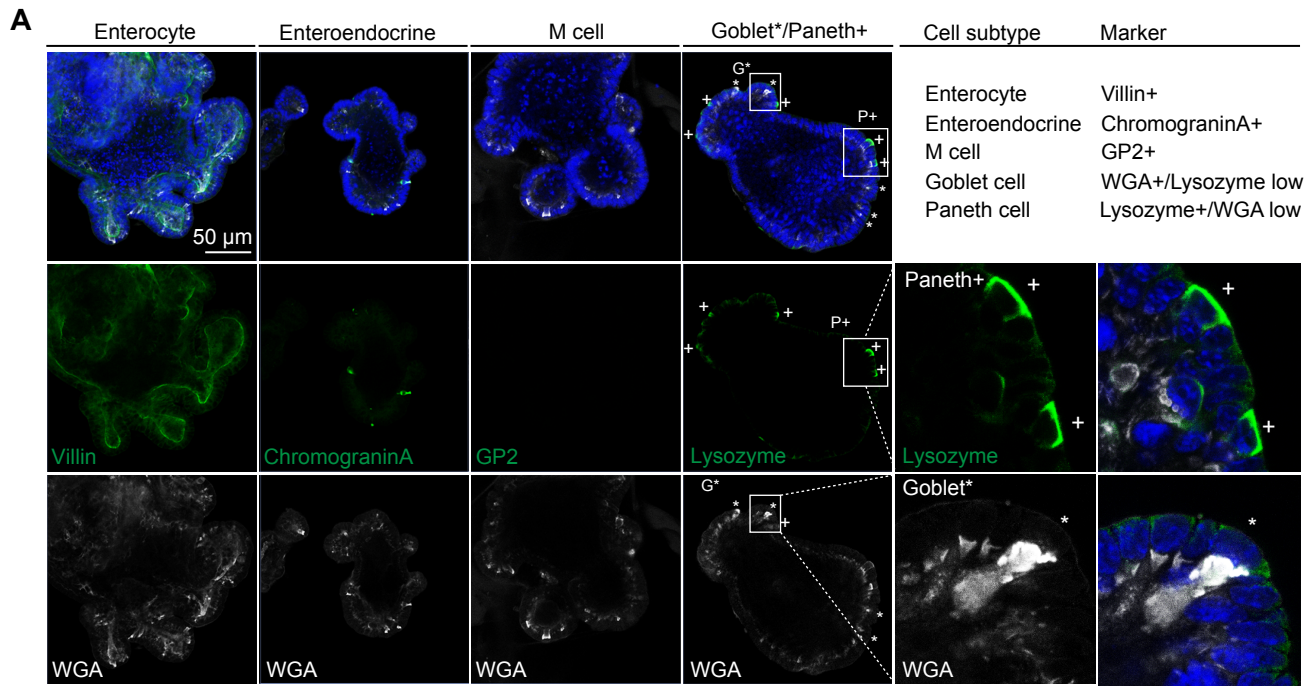
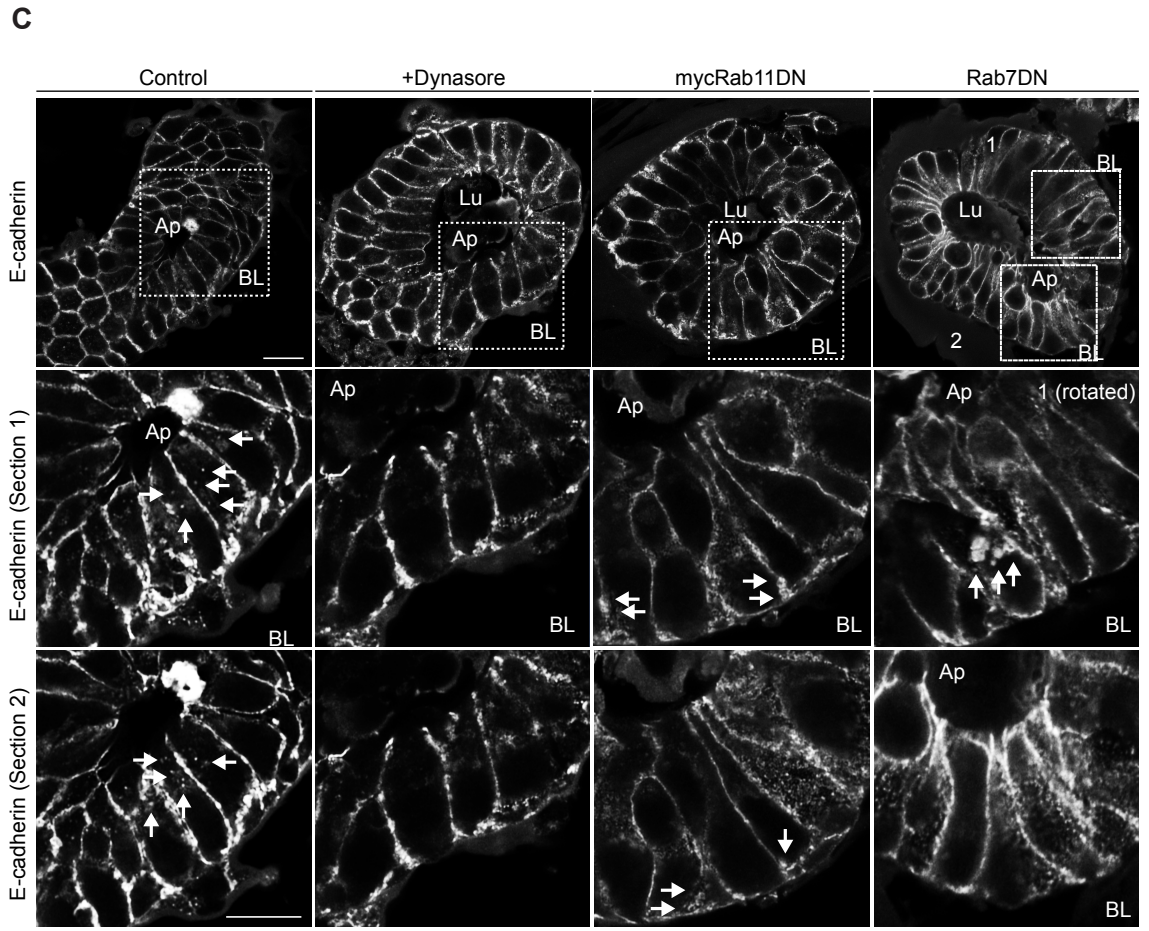
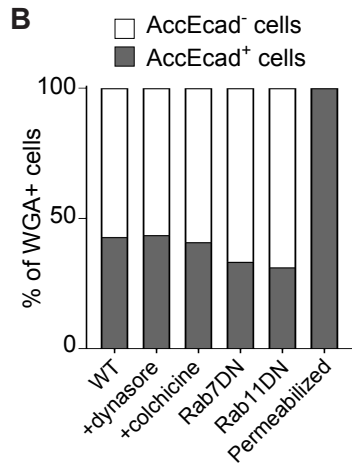
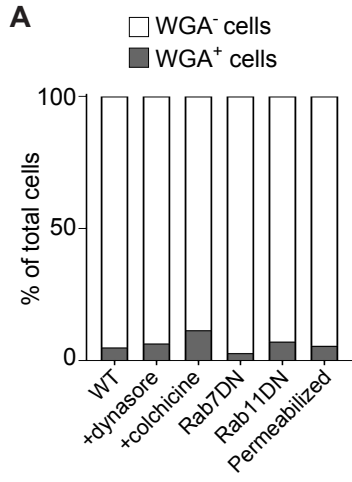


Figure S1. Expression of InlA by *Listeria innocua* allows translocation across the intestinal organoid epithelium. Related to Figure 1.

(A) Cell subtype heterogeneity in organoids. Enterocytes (villin⁺), enteroendocrine cells (chromograninA⁺), goblet cells (WGA⁺/Lysozyme^{low}), Paneth cells (Lysozyme⁺/WGA^{low}) and M cells (GP2⁺) are shown. Note that M cells are absent in intestinal organoids. (B) Goblet cell (arrow) labeled with WGA and cytokeratin-18. Besides the labeling, note that goblet cell displays cup-shaped morphology with apical side opened and/or squeezed nucleus. (C) % of WGA⁺ cell population in *Listeria* non-injected (left, control) and microinjected (right) organoids. Organoids were incubated for 16 hours post microinjection, non-injected control is from the same plate (non-injected neighboring organoids). Two-Way ANOVA test. NS: Not significant; p=0.61. (D) Confocal images of *Li*-GFP(InlA) (arrows) underneath the goblet cells after microinjection. 3D reconstruction and optical sections of boxed area are shown. Mucus material is not visible in the organoids on the right due to the fixation, thus goblet cells (asterisk) are identified based on typical goblet-shaped cellular morphology with opening of its apex. (E) Left: 3D reconstruction of an organoid showing translocated bacteria together with WGA⁺ stained material, indicating that the bacteria exit the goblet cell with the mucus. Center & Right: Optical section of the boxed area on the left. Mucus labeled with WGA that exited along with the bacteria is marked with an arrow.



Listeria (EGD-GFP) injected, 16 h incubation

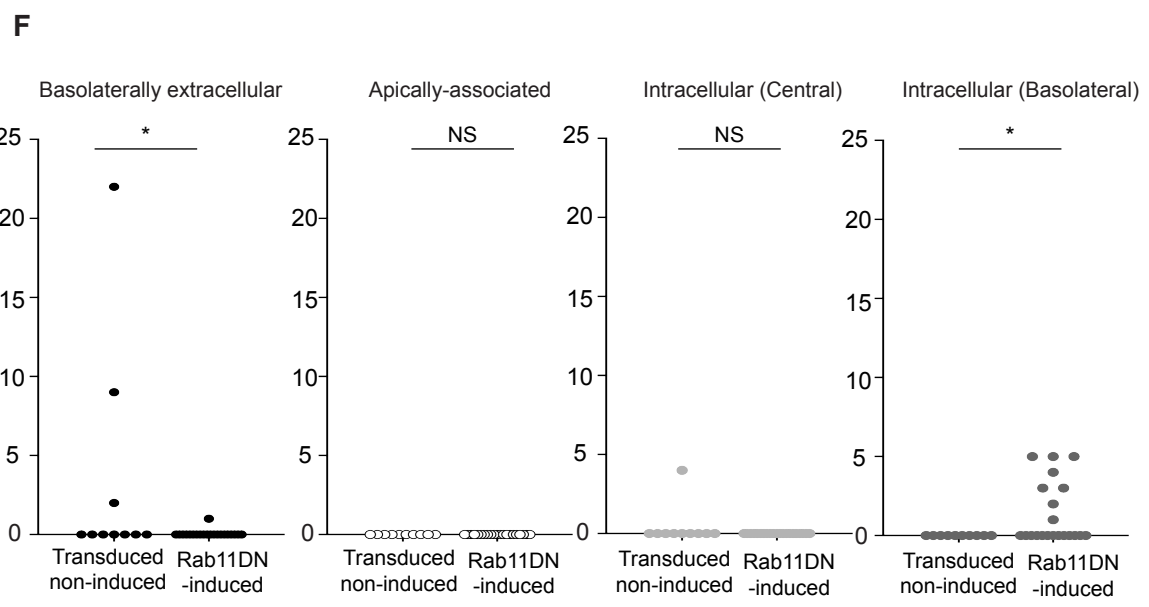
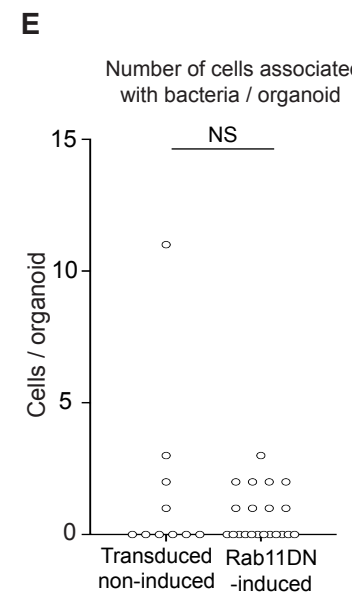
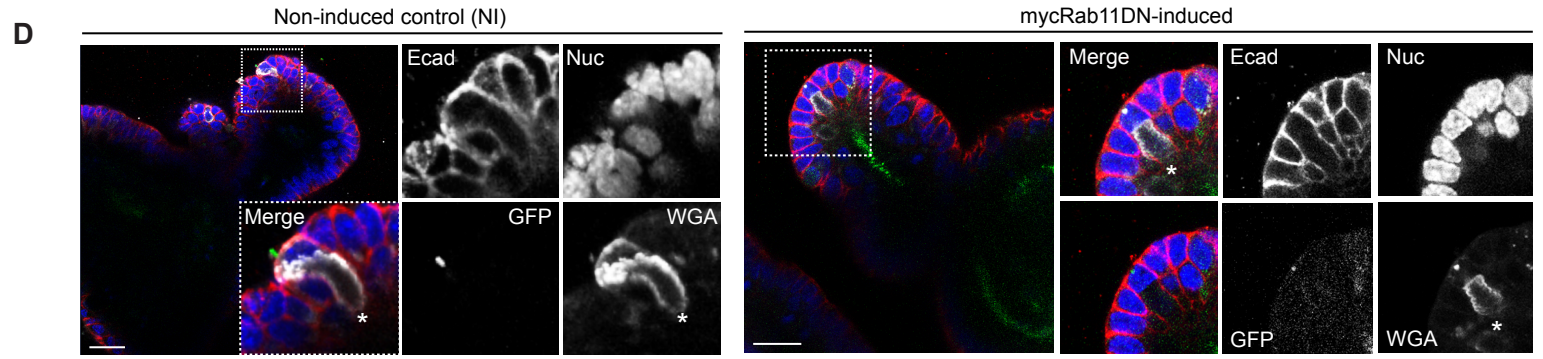
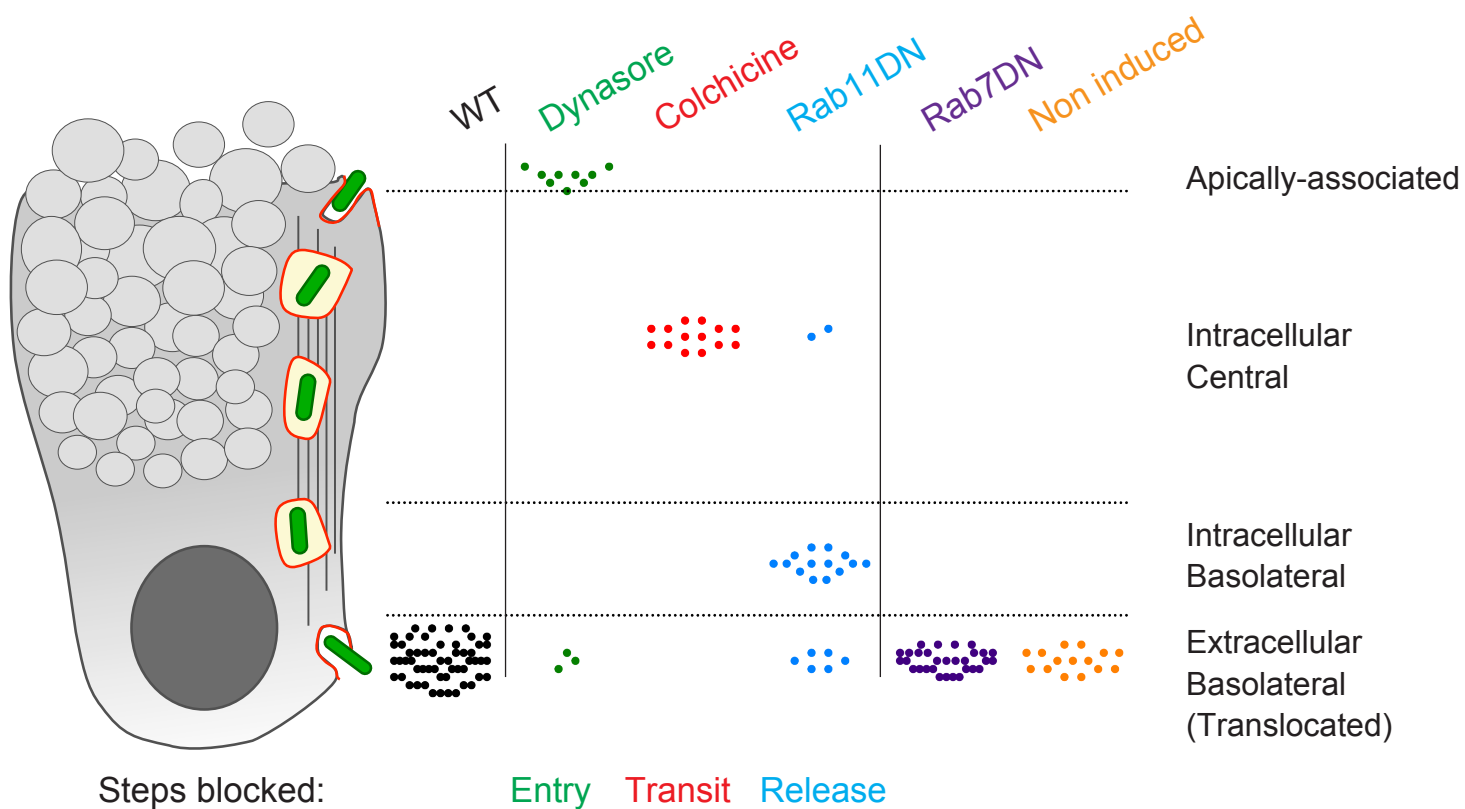


Figure S2. Inhibition of Ecad recycling pathway impairs *Lm* transcytosis. Related to Figure 2, 3 and 4.

(A) % of goblet cells in organoids of indicated settings. Expelled mucus was identified with WGA staining. Organoids were briefly treated with DAPT and IL-13 to partially enrich goblet cell and mucus secretion (Method). (B) Distribution of lumenally accessible Ecad on goblet cells in organoids with indicated treatments. (C) Ecad localization in indicated conditions. In control organoids, Ecad endocytic punctae can be seen in the cytosol (1st column arrow), which is abolished when Dynasore is added (2nd column). Ecad aggregates can be seen in Rab11DN-expressing organoids (3rd column), suggesting that Ecad recycling/release is perturbed. Ecad in Rab7DN-expressing organoids are observed in big cytosolic aggregates (box 1) or dispersed cytosolic punctae (box 2), indicating that Ecad degradation is perturbed. Scale bar, 20 μ m. (D) Organoids microinjected with WT *Listeria* were incubated for 16 hours in presence of doxycycline to induce DN protein. While *Listeria* translocates across the goblet cell in transduced, non-induced control (NI, left), *Listeria* is trapped at the basal pole inside the goblet cell in Rab11DN induced organoids (right). Goblet cells are marked with a star. Scale bar, 20 μ m. (E) Quantification of number of cells associated with bacteria per organoids. Mann-Whitney test. NS: not significant. (F) Quantification of number of bacteria per organoids in indicated location. Counts were performed in 10 non-induced and 21 Rab11DN organoids. Mann-Whitney test. NS: non significant; *: $p < 0.05$.



Difference with WT	Dynasore	Colchicine	Rab11DN	Rab7DN	Non induced
Apically-associated	**	NS	NS	NS	NS
Intracellular Central	NS	****	NS	NS	NS
Intracellular Basolateral	NS	NS	****	NS	NS
Extracellular Translocated	*	**	*	NS	NS

Figure S3. Molecular mechanism involved in *Listeria* transcytosis across the goblet cell.

Related to Figure 2 and 4.

Top: Graphical illustration combining the results of microinjection, with the total number of bacteria counted in each condition of organoids. Rab7DN-induced and transduced but non-induced organoids display basolaterally extracellular bacteria as WT organoids. This indicates that bacteria translocate across the organoid epithelium independently of Rab7-mediated Ecad degradation. Inhibition of dynamin-mediated endocytosis in organoids by dynasore leads to significantly increased number of bacteria that are apically associated to the goblet cells, but significant decrease in the number of translocated bacteria. This indicates that Ecad endocytosis is involved in the step of bacterial entry. Microtubule dynamics inhibition by colchicine also leads to significant decrease of translocated bacteria counts, but significant increase of intracellular bacteria that are located near the center of the cells. This indicates that bacteria-containing vesicles transit *via* microtubule within the goblet cells. Rab11DN-induced organoids show significant increase in the number of intracellular bacteria located in the basolateral area of goblet cells, but significant decrease in the number of bacteria elsewhere, suggesting that functional Rab11 is required in completing bacterial translocation. **Bottom:** Table summarizing the statistical significances. Kruskal Wallis test. Comparison to WT. NS: Not significant; *: $p < 0.05$; **: $p < 0.01$; ****: $p < 0.0001$